Experimental and Scale-span Numerical Investigations in Conventional and Longitudinal Torsional Coupled Rotary Ultrasonic Assisted Drilling of CFRPs

Yong Liu (liuyong.1991.happy@nuaa.edu.cn)
Jiangsu University of Science and Technology
Qiannan Li
Jiangsu University of Science and Technology
Zhenchao Qi
Nanjing University of Aeronautics and Astronautics
Wenliang Chen
Nanjing University of Aeronautics and Astronautics

Research Article

Keywords: CFRPs, Drilling, Scale-Span, LTC-RUAD, Ultrasonic vibration amplitude

Posted Date: May 25th, 2021

DOI: https://doi.org/10.21203/rs.3.rs-537841/v1

Version of Record: A version of this preprint was published at The International Journal of Advanced Manufacturing Technology on November 29th, 2021. See the published version at https://doi.org/10.1007/s00170-021-08286-7.

Experimental and scale-span numerical investigations in conventional and longitudinal torsional coupled rotary ultrasonic assisted drilling of CFRPs

Yong Liu[1,2*], Qiannan Li[1], Zhenchao Qi[2*], Wenliang Chen[2]

[1]College of Mechanical Engineering, Jiangsu University of Science and Technology, Zhenjiang, 212003, PR China

[2]College of Mechanical and Electrical Engineering, Nanjing University of Aeronautics and Astronautics, Nanjing, 210016, PR China.

*Corresponding author: Yong Liu, E-mail address: liuyong.1991.happy@just.edu.cn.

Zhenchao Qi, E-mail address: qizhenchao2007@foxmail.com.

Abstract

Longitudinal torsional coupled rotary ultrasonic assisted drilling (LTC-RUAD) technology is introduced to improve the surface roughness of the hole wall and solve the tear, burr and delamination of carbon fiber reinforced polymers (CFRPs) induced by large thrust force and torque during conventional drilling (CD). An experiment and scale-span numerical investigation of drilling CFRPs was presented for both CD and LTC-RUAD process in this study. A drilling experimental platform using LTC-RUAD was built via a novel independently designed and manufactured LTC-RUAD vibration actuator, while the drilling experiments involving T700S-12K/YP-H26 CFRPs specimens with different process parameters were carried out by adopting the different ultrasonic vibration amplitude (UVA) in the longitudinal and torsional directions. Then, a three-dimensional (3D) scale-span FE simulation model of CD and LTC-RUAD which applied the different UVA using tapered drill-reamer (TDR) are developed to find more details about the effects of machining quality of the holes. Experimental and simulation results revealed that the maximum average thrust force reduction is observed to be as high as 30% under certain drilling conditions, and the maximum average thrust force and the delamination factor of the drilled hole shows a "concave" trend with the increase of the UVA. The quality at the exit of the drilled hole is the best when adopting S_r=2000rpm, S_f=0.01mm/rev, A_{lon}=7.02μm and A_{tor}=9.29μm in LTC-RUAD. The delamination factor is only 0.054. The damage factors are reduced by 69.67% compared with CD.

Keywords:

CFRPs; Drilling; Scale-Span; LTC-RUAD; Ultrasonic vibration amplitude

1.Introduction

Carbon fiber reinforced polymers (CFRPs) are being widely used in aerospace industry and automobile industries and several other structural applications owing to their superior mechanical and physical properties [1,2]. Through a near-net shape process is usually for CFRPs components, but additional machining operations are often required to facilitate furtherly installation of rivets or bolted joints. For any mechanical fastening, conventional drilling (CD) process is extensively used for producing CFRPs holes. However, different to drill metal materials, various mechanical damage in terms of delamination, poor surface integrity, fiber pullout, fiber breakage and burr usually occur due to the heterogeneous and anisotropic nature of CFRPs laminates during drilling [3,4]. These undesirable drilling-induced damages not only directly deteriorate the surface finish and assembly tolerance, but also reduce the hole strength against fatigue, thus the load-carrying capacity of CFRPs structure is affected [5]. To overcome the aforementioned problems, a need for a less invasive drilling technique capable to mitigate damage in drilling CFRPs structural components is recognized.

A hybrid non-traditional process, known as “rotary ultrasonic assisted drilling (RUAD)”, has been successfully extended to the area of CFRPs drilling owing to its remarkable improvement in machinability for machining difficult-to-machine metal material in the last few years [6,7]. In RUAD, high frequency vibrations, typically in the range of 20kHz, generated by a piezoelectric transducer are superimposed on a rotating standard tool in the axial direction or rational direction to improve the machining process. Fundamentally, RUAD is a completely different process from CD, and the tool-workpiece interaction is intermittent with significantly higher deformation rates. Nonetheless, the cutting process is continuous in CD. Compared with CD, RUAD is shown to be beneficial for drilling holes in brittle materials [8] and has many documented advantages, for instance, reduction in thrust force, improved surface finish, better hole quality, elimination of burrs and lower tool wear [9].

In the literature, some researchers have conducted RUAD experiments to investigate the effect of different drill bit geometries, different process parameters on damage defects of the drilled holes. Sadek et al. [10] investigated the RUAD process to reduce thermal and mechanical defects associated with drilling of CFRPs, the results revealed that the optimized RUAD condition can reduce the machining temperature by 50%, the thrust force by 40% and produce delamination-free holes,

without affecting productivity. Cong et al. [11] employed the similar RUAD method to drill CFRPs laminate to prevent clog and improve the hole's quality. Wang et al.[12,13] also successfully extended RUAD method in which vibration is applied along the tool axis to improve the machining of the CFRPs surfaces, whereas the risk of delamination damage increases since the cooling fluid with a certain pressure is pumped through core drill. Thomas et al.[14] investigated the drill bit's vibrational characteristic, the experimental and simulation results showed that there are several well-documented advantages of RUAD over CD techniques such as reduction in thrust forces and torque, better surface finish, low tool wear and elimination/reduction in burr formation. Makhdum et al. [15] conducted an extensive experiment by using high-frequency vibration to excite a drill bit during its standard operation to study the effect of RUAD on CFRPs, the research results showed that adopting RUAD technique had a significant improvement to improve the drilling quality compared with CD. Asami et al. [16] developed a LTC vibration device for the ultrasonic machining of brittle materials with an abrasive slurry. Compared with the one-dimensional longitudinal vibration drilling, the LTC vibration was discovered to improve the machining efficiency. These above studies showed that there are several advantages of RUAD over CD such as reduction in drilling forces and torque, better surface finish, low tool wear and elimination in burr formation.

Although experimental efforts have been done about the use of RUAD in the drilling of CFRPs, still some considerable works remain so that this strategy can be industrialized, efficiently. Accordingly, finite element (FE) simulation is a helpful approach to evaluate this machining process in detail [17]. Expect for few literatures reported by Phadnis et al.[18,19] in simulation of cutting forces in RUAD, there are not any corresponding research representing burr formation, delamination generation, as well as tool movement in the simulation of vibration drilling owing to the complexity involved in modeling of such processes and the extent of computational resources required. In the aforementioned studies, they indicated that the average thrust force in RUAD was reduced as high as 30% compared to CD of CFRPs. Furthermore, it was noted that the predicted results were in good agreement with experimental results.

However, in the numerical analysis for CFRPs drilling using RUAD, almost all of them used macro-mechanics theories (Tsai-Wu [20], Hashin [21,22], Puck [23] and Chang-Chang [24], etc.) although they were capable to determine the damage modes

by regarding composite as homogeneous material, where some real damage defects are impossible to be simulated, such as burr, etc. In addition, CFRPs is a kind of multiphase material with macro-micro characteristic, whereas these theories did not consider the influence of local stress difference caused by different mechanical performances of constituent fiber and matrix, which are related to the behaviors of CFRPs at macroscale. For the drilling FE model, the stress and strain of the CFRPs laminate in the direction of thickness, which is lacked of considering in these macro-mechanics theories, should be considered in particular. If the micro-scale modeling method of the CFRPs FE model is adopted, which is limited by computing power and efficiency in a high-performance workstation.

Meanwhile, as one of the two major variables of RUAD, ultrasonic vibration amplitude (UVA) in the longitudinal and torsional direction plays a dominate role in the longitudinal torsional coupled rotary ultrasonic assisted drilling (LTC-RUAD) process. The influence of machining quality of the holes is not researched furtherly as the change of the UVA. Plentiful studies are major focused on “abrasive drilling” in terms of optimizing the process parameters, whereas the drilling and grinding coupled process in the drilling of CFRPs is not researched further. For instance, a tapered drill-reamer (TDR) or step drill bit are adopted in the LTC-RUAD process for CFRPs drilling.

Thus, this study presents an experiment and scale-span numerical investigation of drilling in a CFRPs for both CD and LTC-RUAD process by modifying the different UVA in the longitudinal and torsional direction. First, a drilling experimental platform is built based on the novel independently designed and manufactured LTC-RUAD vibration actuator, while drilling experiments involving T700S-12K/YP-H26 CFRPs specimens with different process parameters are carried out via modifying the UVA in the longitudinal and torsional directions. Meanwhile, a three-dimensional (3D) scale-span FE simulation model of CD and LTC-RUAD which applied the different UVA using TDR are developed to find more details about the effects of machining quality of the holes. Finally, the defect suppression mechanism of CFRPs hole in LTC-RUAD is revealed via the FE simulation results from the perspectives of the thrust force and torque, burr and delamination at the hole exit. In addition, the correlative factors affecting the hole making quality, hole making defects and cutting force of CFRPs to optimize the process parameters and LTC parameters, which is conducive to achieve high-precision drilling.

2. Experimental set-up and conditions

2.1 LTC-RUAD test system and calibration

The LTC-RUAD experimental instruments used in this paper is attributed to be independently designed and manufactured by Nanjing University of Aeronautics and Astronautics. The whole LTC-RUAD test system consists of a BT40 LTC ultrasonic vibration holder, a labview controller, a power supply and the corresponding voltage amplifier. LTC ultrasonic vibration holder majorly comprises of longitudinal torsional coupler, electrode slice, piezoelectric ceramic piece and amplitude amplifier pole, etc. The actual parts and connection relationship of each parts are shown in Fig.1.

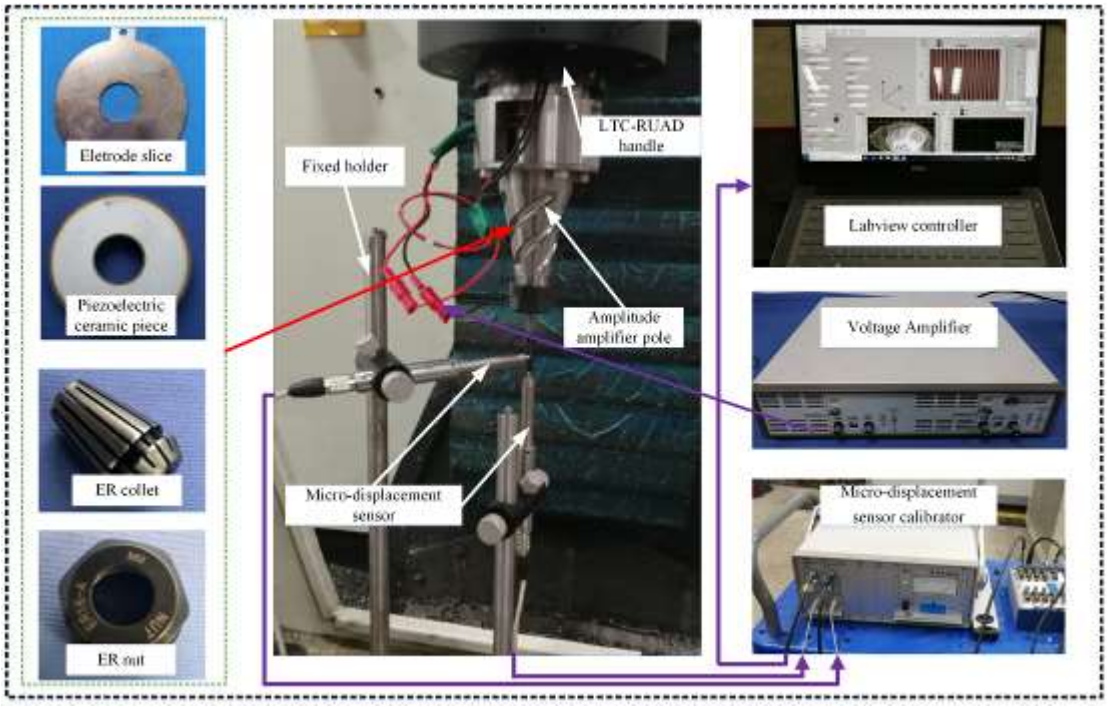

Fig.1 LTC-RUAD handle and ultrasonic amplitude calibration

Before the experiment, it is necessary to calibrate the amplitude and resonant frequency of longitudinal and torsional vibration of the cutter according to the extended length of the TDR bit. The resonance frequency of the LTC experimental system is calibrated at the initial voltage, and different voltages are applied to the tool handle to control the different UVA. As shown in Fig.1, the calibration process of longitudinal and torsional amplitudes is completed by real-time monitoring of micro-displacement sensor which produced by HangZhou Oriental Gauge Technology Co., Ltd.

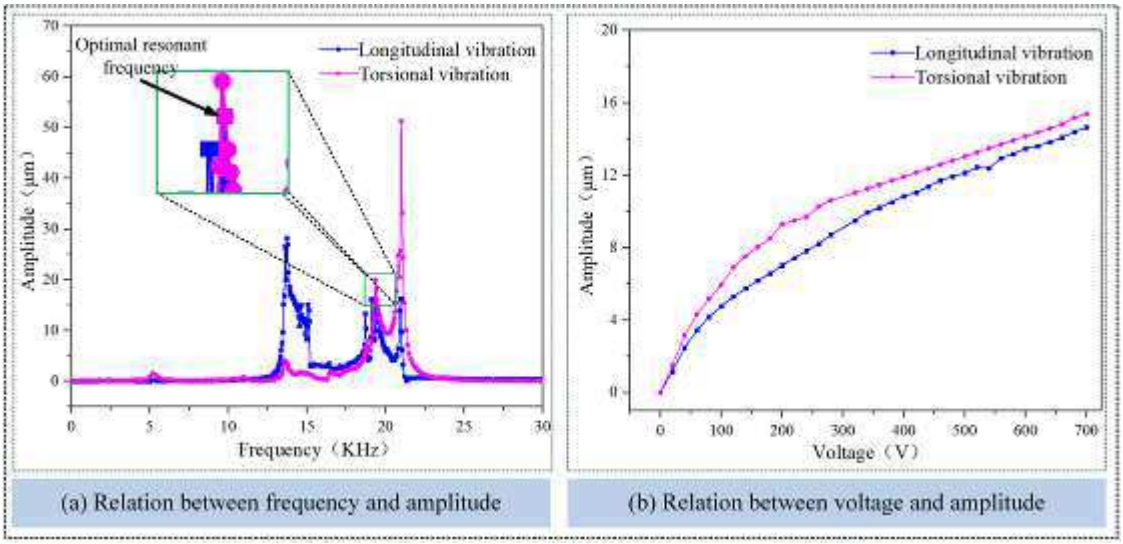

Fig.2 Frequency-amplitude and voltage-amplitude diagram

Fig.2 presents the amplitude change curves of the TDR bit in the longitudinal and torsional directions at different frequencies and voltages when the length of the transverse blade from the ER nut is approximately 40mm. The resonant frequencies of longitudinal and torsional amplitudes are not consistent under the different voltages, and the resonance amplitudes are larger in longitudinal and torsional directions when the frequency is about 19.6 kHz, as shown in Fig.2(a). Simultaneously, the amplitude of longitudinal vibration and torsional vibration shows a semi-linear relationship at the resonant frequency, and it's different from the original design which is supposed to be linear, as shown in Fig.2(b). The primary reason for such errors is that the piezoelectric ceramic piece has hysteresis and creep properties, etc.

2.2 LTC-RUAD experimental procedure of drilling CFRPs laminate

A corresponding CFRPs with a thickness of 5.76 mm (32 layers) was used for conducting the drilling experiments in this study. The CFRPs were made using unidirectional prepregs supplied by GW composite Co, Ltd, and the model of prepregs was T700S-12K/YP-H26. The curing process mainly followed the literature [25]. The fiber volume fraction after curing was approximately 59%. The entire curing process was performed in the composite material forming laboratory of Nanjing University of Aeronautics and Astronautics. After curing, the CFRPs were made into the dimension of the drilling specimen via waterjet cutting, for which the length and width of specimens were 180 mm and 120 mm, respectively.

The entire schematic diagram of the experimental setup and the specific experimental setup are illustrated in Fig.3 and Fig.4. It mainly consists of an LTC-RUAD system and a data acquisition system. The CFRPs were mounted on a

dynamometer using a special fixture on the table of a XK7124 CNC machining center, and the TDR bit which is installed on the LTC-RUAD handle was fed into the CFRPs. Drilling experiments were carried out on CFRPs using a diameter Φ 6 mm cemented carbide TDR bit. Experiments were conducted without coolant. The thrust force during drilling was measured by using a piezo-electric dynamometer (type Kistler 9257B). The charge amplifier (type Kistler 5407A) converted the resulting charge signals, which were proportional to the force, to voltage and managed the experiment through the data acquisition system (type NI DAQ).

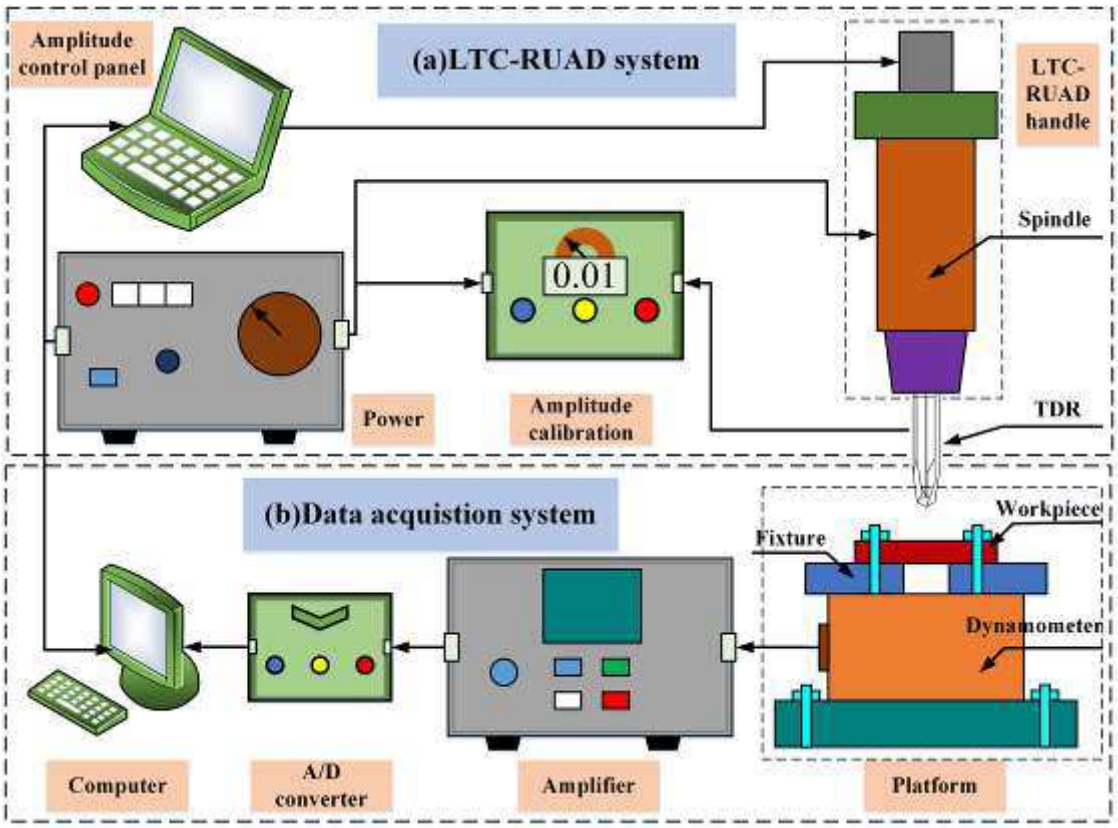

Fig.3 Schematic diagram of LTC- RUAD experimental setup

A full factorial design of experiments with two factors based on the initial process parameters was adopted in this study [26]. Three levels of spindle feed rate and their corresponding spindle rotation speed were employed. According to the amplitude of the calibration curve which is shown in Fig.2, the torsional UVA and longitudinal UVA were corresponding to each other under the same voltage owing to the resonance amplitude was inspired by the same piezoelectric ceramic piece. Therefore, the different UVA generated under different voltages were adopted according to the optimal resonant frequency of the LTC-RUAD handle. The integrated machining scheme is shown in Tab.1.

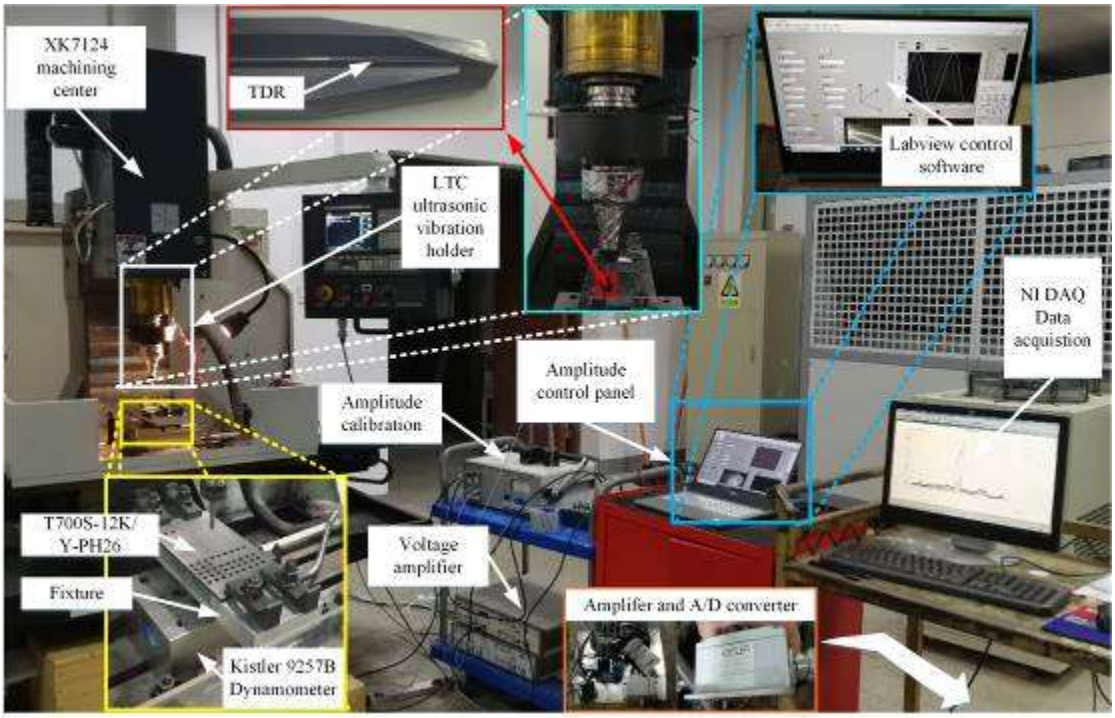

Fig.4 LTC-RUAD experimental setup for drilling T700S-12K/Y-PH26

Tab.1 Machining scheme

Parameters	CD	LTC-RUAD
Drilling depth (mm)	20	20
Spindle rotation speed(rpm)	2000、3000、4000	2000、3000、4000
Spindle feed rate(mm/rev)	0.01、0.02、0.03	0.01、0.02、0.03
Resonance frequency (KHz)	0	19.6
The UVA of longitudinal vibration A_{lon} (μm)	0	4.77、6.14、7.02、7.81、9.63、10.14
The UVA of torsional vibration A_{tor} (μm)	0	5.94、7.88、9.29、9.62、10.73、11.21

Experiments of each machining parameter were repeated 3 times to obtain a satisfactory measured dataset. All the experiments were carried out on the LTC-RUAD handle. For instance, the voltage was 0 *V* in CD. In addition, a new TDR bit was employed for the sake of removing the influence of tool wear during drilling. All process experiments were performed using three laminates. Finally, as shown in Fig.12, the hole's damage of the CFRPs specimens was observed through a scanning electron microscope (SEM) produced by HiROX Co. Ltd after waterjet cutting, such as delamination and burr, etc.

3.Scale-span finite element analysis of drilling in CFRPs using LTC-RUAD

3.1 Principle of the LTC-RUAD process of CFRPs using TDR

The structure of TDR mainly contains three parts: chisel edge, first cutting edge and secondary cutting edge [27]. The cutting process of the bit is rotary and the feed motion is located at the axial direction in the CD of CFRPs, respectively. The first cutting edge is the drilling process that is mainly to achieve material removal, while the second cutting edge is the grinding process which would achieve the role of reaming. The thrust force is mainly determined by chisel edge owing to the chisel edge squeezes the workpieces during drilling, and the torque is generated by the first and secondary cutting edge according to the cutting thickness of the single rotary.

In LTC-RUAD, the LTC vibration of the TDR bit for hole drilling of the CFRPs is applied. Fig.5(a) shows the kinematic view of the LTC-RUAD. Clearly, a polar coordinate is defined on the TDR bit end face. The moving trajectory of position r from the center of the TDR can be written as follows.

$$\begin{cases} L = -A_{tor}\sin(2\pi ft) - 2\pi r S_r t \\ R = r \\ Z = -A_{lon}\sin(2\pi ft) - S_f\left[2\pi f A_{tor}\cos(2\pi ft) + S_r\right]t \end{cases} \tag{1}$$

where L, R and Z denote the kinematic position of the drilling. A_{tor} and A_{lon} denote the UVA of torsional vibration and longitudinal vibration, respectively. The parameter f denotes the ultrasonic frequency, t denotes the time, r denotes the displacement from the center of the TDR, S_r denotes rotational speed due to the TDR ration, and S_f denotes the feed rate of the TDR.

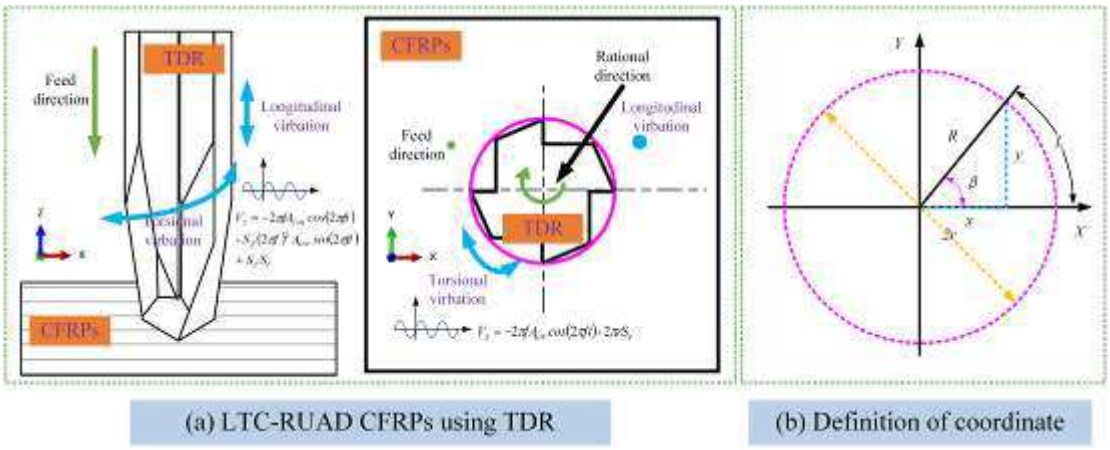

Fig.5 Illustration of LTC-RUAD using TDR

Simultaneously, as showed in Fig.5(b), the circumferential angular displacement β of the TDR can be written as.

$$\beta = L / r \tag{2}$$

The displacements at each point in TDR can be expressed as

$$\begin{cases} x = r * cos\left[\left(-A_{tor}\, sin\left(2\pi ft\right) - 2\pi r S_r t\right) / r\right] \\ y = r * sin\left[\left(-A_{tor}\, sin\left(2\pi ft\right) - 2\pi r S_r t\right) / r\right] \\ z = -A_{lon}\, sin\left(2\pi ft\right) - S_f\left[\left(2\pi f A_{tor}\, cos\left(2\pi ft\right) + S_r\right)\right]t \end{cases} \tag{3}$$

where x, y and z denote the displacement in rectangle coordinate, respectively.

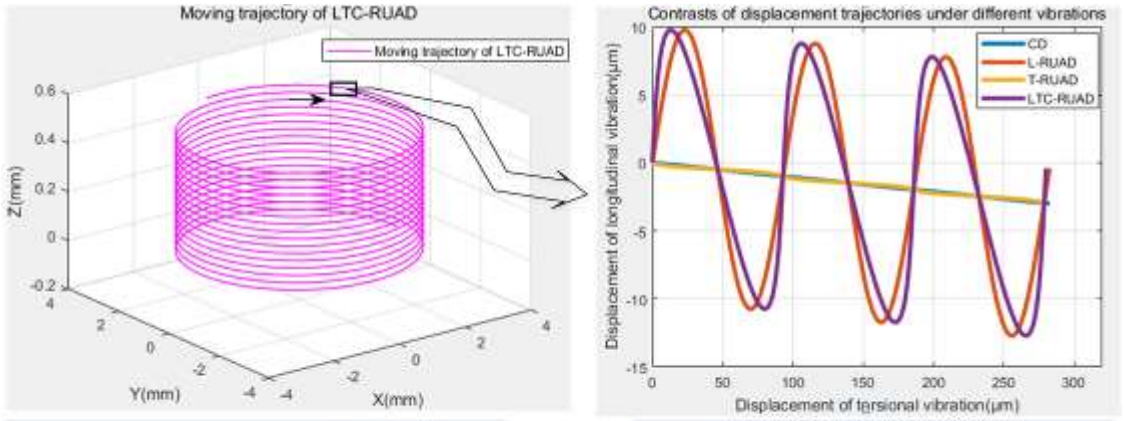

(a) Moving trajectory of LTC-RUAD

(b) Contrasts of displacement trajectories under different vibrations mode

Fig.6 Moving trajectory of TDR

Fig.6(a) presents the calculated moving trajectory of the position r from the center of the TDR when r=3mm, S_r=2000rpm, S_f=0.01mm/rev, A_{tor}=10μm, A_{lon}=10μm, f=19.6KHz. Fig.6(b) demonstrates that the moving trajectory of the TDR in LTC-RUAD (purple line) is rather different from the moving trajectory in the CD (blue line), longitudinal RUAD (orange line) and torsional RUAD (saffron yellow line) owing to the torsional vibration and longitudinal vibration of the tool. There are reciprocating effects in the axial and rotational directions when adopts the LTC-RUAD process, which means that the tool will lift and do not contact the material within a rotation period. The cure also indicates that the chip thickness of the cutting edge is not uniform, while the fibers can be cut off more quickly in the cutting direction. Besides, the softening of resin is promoted due to the reciprocating microscopic cutting, so that the surface topography of the hole may appear the obvious ironing phenomenon. Thus, the moving trajectory difference of the TDR in CD and LTC-RUAD would highly affect the corresponding machining performances.

3.2 Progressive failure theories of the scale-span model of CFRPs

Since the integrate FE analysis process is clearly explained in previous studies [28], the main points are only briefly reviewed to the scale-span analysis method in

this study. The adopted modeling method in this paper is based on the implementation of the dynamic micromechanics of failure (MMF) criterion of CFRPs. The kernel of this method consists of establishing the damage-failure constitutions of fiber and matrix under dynamic loading conditions and realizing damage-failure information interaction between the representative volume element (RVE) model which includes fiber and matrix and the macroscopic drilling FE model of CFRPs. According to the scale-span FE drilling schematic diagram which is shown in Fig.7, the whole simulation process is mainly divided into three steps:

Step (1): The components of CFRPs are simplified as idealized multi-directional pre-set lay-up sequence structure which includes multilayer UD-CFRPs. It is assumed that the structure of multi-directional CFRPs (MD-CFRPs) is flawless and that the fibers and matrix are tightly bonded during curing. Some minor defects in the material are overlook, such as voids and micro-crack, which is shown in Fig.7 (c). Meanwhile, the drilling bit FE model is also required to be established according to the actual drilling conditions, which is shown in Fig.7 (a).

Step (2): The corresponding RVE model is also established via the basic parameter of CFRPs, such as the diameter of the filament fiber and the fiber volume fraction of CFRPs, etc. which is shown in Fig.7 (b). The stress-strain relationship of the damage element of the macroscopic FE model of CFRPs will be transferred to the RVE model via SAFs when the bit is in contact with CFRPs. These elements of fiber and matrix in RVE model will be secondary analyzed through the MMF criterion of CFRPs, including element failure judgement, stiffness degradation and deletion, etc. In addition, if the elements are not deleted in the current increment, the element with reduced stiffness will be homogenized in macroscopic drilling FE model, and the macroscopic elastic properties of elements are characterized by the scale-span prediction method [29], which is used for analysis in the next iteration step.

Step (3): The macroscopic elastic properties of elements which have different degrees of damage will be assigned to the corresponding macroscopic elements with different lay-up sequence structure of CFRPs. Then, the next iteration analysis of the macroscopic drilling FE model will be carried out, and the scale-span simulation process of drilling CFRPs will be end if the pre-set increments is reached.

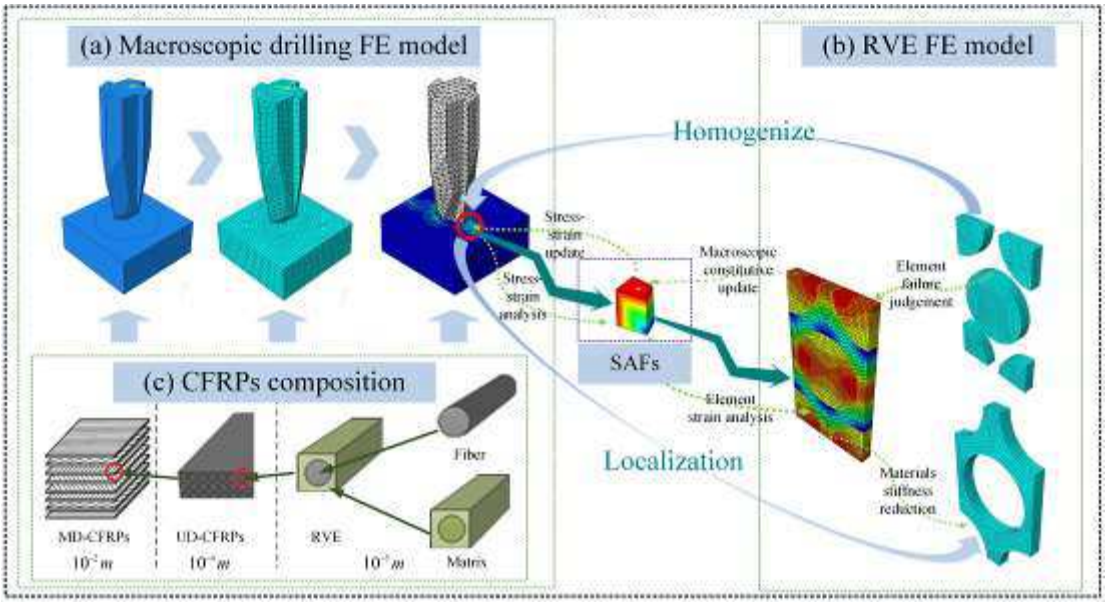

Fig.7 Scale-span FE drilling schematic diagram

3.3 Drilling scale-span FE modelling of CFRPs using LTC-RUAD

A 3D drilling FE model of corresponding CFRPs was established with the help of the ABAQUS/Explicit software. The dynamic characteristics of the entire drilling process accounting for the complex contact interaction between the TDR and CFRPs' surface was characterized in the FE model. The newly developed 3D progressive damage failure model based on the MMF criterion explained in the literature [28] were used as user-defined material model for CFRPs to facilitate element deletion of mesh elements and simulate inter-ply delamination which suffered severe deformations. The corresponding span-scale FE model of drilling CFRPs and the parameters of the TDR are shown in Fig.8.

High temperature-resistant CFRPs (type T700S-12K/YP-H26), which is the same type of composites that used in the experiment, are used as the research object in the FE modeling. The fiber volume fraction is approximately 59%, and the layup sequence of the CFRPs is $[(0°/90°/45°/-45°)s]_2$. Orthotropic material property was assigned to each UD-CFRPs laminate according to the fiber orientation by using a predefined local coordinate system. The cohesive elements (CEs) [28], which is modeled as having a thickness 0 mm, was used for simulating the delamination phenomenon. The materials parameters of UD-CFRPs laminate elements and cohesive-zone elements are reported in Tab.2 and Tab.3, respectively.

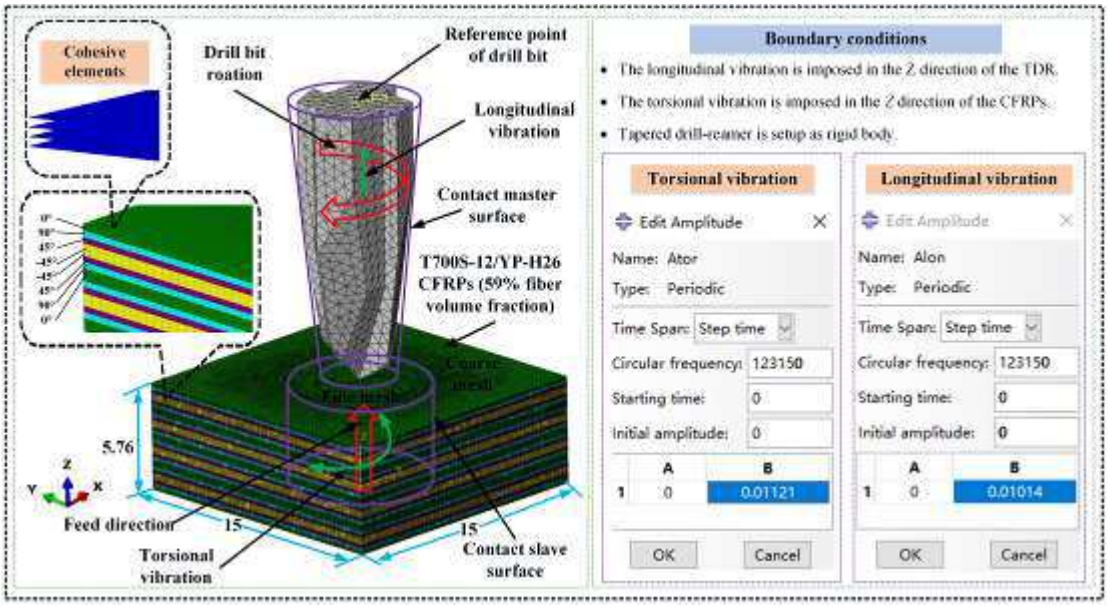

Fig.8 Setup showing the FE model of drilling CFRPs using LTC-RUAD

Tab.2 Material parameters used to model unidirectional CFRPs laminate elements

Elastic parameters	Value (GPa)	Strength parameters	Value (GPa)
E_1	138.7	X^T/X^C	1870/1026
E_2=E_3	7.04	Y^T/Y^C	45/156
v_{12}=v_{13}	0.25	Z^T/Z^C	40/145
v_{23}	0.31	S_{XY}	87
G_{12}=G_{13}	2.959	S_{XZ}	87
G_{23}	2.505	S_{YZ}	58

Tab.3 Material parameters used to model interface CEs

Stiffness	Value (N/mm^3)	Strength parameters	Value (MPa)	Fraction energy	Value (N/mm)
K_n	4×10^6	δ_n	60	G_n	0.2
K_s=K_t	1×10^6	δ_s=δ_t	90	G_s=G_t	1

The overall dimensions (15 mm×15 mm×5.76 mm) of the laminated plate were modelled as CFRPs with an individual ply thickness of 0.18mm. A cemented carbide (K40) with coated TDR of diameter Φ 6 mm was modeled as a discrete rigid body to improve the computational efficiency required to discretize the complex bit geometry. A lumped mass and rotary inertia were applied at a reference point located at the top of the TDR bit for the sake of accounting for the thrust force of the entire drilling

process. The reference point of the TDR was also assigned with a single node mass and rotary inertia element, where the axial velocity and rotations were loaded. A refined mesh was used in the immediate vicinity of the model volume to be drilled and a coarse mesh was used to discretize the volume away from the drilling zone for the sake of ensuring that the prediction of thrust force was more accurate and maximized utilization of the available computing resources during drilling. The CFRPs were modeled using the C3D8R 8-node, 3D brick reduced integration elements. The cohesive-zone was modeled using the COH3D8 0-thickness CEs. Analogously, the TDR was modeled with the C3D10M 10-node, 3D discrete rigid elements. The whole FE model consisted of 3382122 elements, including 819108 CEs and 8208 tetrahedral elements in the model of the TDR, with the smallest element size of 40 μm.

As the limited by the degree of the freedom in the boundary condition set module of the ABAUQS software, the process parameters and LTC ultrasonic vibration parameters are required to setup separately, which is a little different from the actual working conditions. Velocity boundary conditions were used to account for dynamic characteristics of the entire drilling process. The spindle rotation was loaded at the reference point located at the top of the TDR, namely the rotational motion is rotating around about the *Z* direction. Meanwhile, the reference point was constrained in the *X* and *Y* directions, and the longitudinal vibration was imposed in the *Z* direction. Similarly, the feed rate was loaded at the CFRPs workpiece, and the torsional vibration was imposed in the *Z* direction. The simulation machining scheme is consistent with the experimental machining scheme. For instance, the settings of the LTC parameters in ABAQUS software is shown in Fig.8 when the resonant frequency is 19.6 kHz, the torsional UVA is 11.21μm and the longitudinal UVA is 10.14μm.

A coulomb friction model was deemed appropriate, and the corresponding coefficient of friction of 0.3 was used in the FE model to analyze frictional effects during drilling simulation. A type of surface-to-surface kinematic contact algorithm in ABAQUS/Explicit was employed to model penalty friction which based interaction between the TDR and CFRPs model. The surfaces of the TDR were set to the master surface and elements that were located in a circular area with a diameter of approximately 10 mm at the center of the CFRPs was assumed to be the slave surface to save computation time.

Based on the aforementioned settings, jobs were created and the corresponding

calculation input file was output to check for errors. The mass scaling factor was set to 10^3 according to the reference [30] to improve computational efficiency on the premise of ensuring accuracy through many attempts. The complete computation of a job required approximately 192 hours on a high-performance computer with two 48 core 8160 platinum processors and 128 GB RAM. All simulations were performed at the high-performance computing facility at Nanjing University of Aeronautics and Astronautics.

4.Results and discussion

For the sake of allowing a better comparison of the experimental and simulated thrust force, torque and the damage in entrance, hole-wall and exit of the performed hole using CD and LTC-RUAD, a typical feed rate of S_f=0.03mm/rev was chosen from the experimental feed data with a spindle speed S_r=2000rpm. Meanwhile, the LTC-RUAD experimental results of other process parameters were also adopted to further evaluate the correctness of the simulation results from the maximum average thrust force, torque and delamination factor, etc.

4.1 Thrust force and torque

Fig.9 shows the experimental and simulated data for the thrust force in drilling of T700S-12K/YP-H26 CFRPs laminate using CD and LTC-RUAD. Apparently, the thrust force and torque prediction results of the drilling FE model are closely corresponding with experiments in the eight stages according to the effects between TDR and CFRPs. The variation trend is almost consistent with the comparison of CD owing to the same initial process parameters are adopted during drilling using LTC-RUAD. Nonetheless, at the same period, there is a great difference in the transient amplitude of variation change $\triangle F$ even though the maximum value is greater than that adopts CD according to the experimental results using LTC-RUAD. The overriding reason is that the cutting process exists impact characteristics at the micro-scale level according to the analysis of the principle of the LTC-RUAD process of CFRPs using TDR, which helps to reduce the fracture toughness of fibers in the contact area, and then can cut them off quickly. Meanwhile, in the scale-span FE model, the elements where is located in contact area are occurred to failure rapidly and will be deleted, and the deleted elements is unrecoverable. Compared with the LTC-RUAD experimental results, the variation of instantaneous thrust force and its amplitude is smaller, whereas the maximum average thrust force is also smaller in the

scale-span FE model. Nevertheless, the vibration amplitude of the scale-span model is smaller than that of the experimental results because of the differences between the scale-span FE model and the microscopic cutting model. For instance, the transient amplitude of variation change $\triangle F\approx 60$N in LTC-RUAD experiment, whereas the$\triangle F\approx 45$N in the corresponding scale-span FE model when the A_{tor}=10.14μm, A_{lon}=11.21μm, as shown in Fig.9(b).

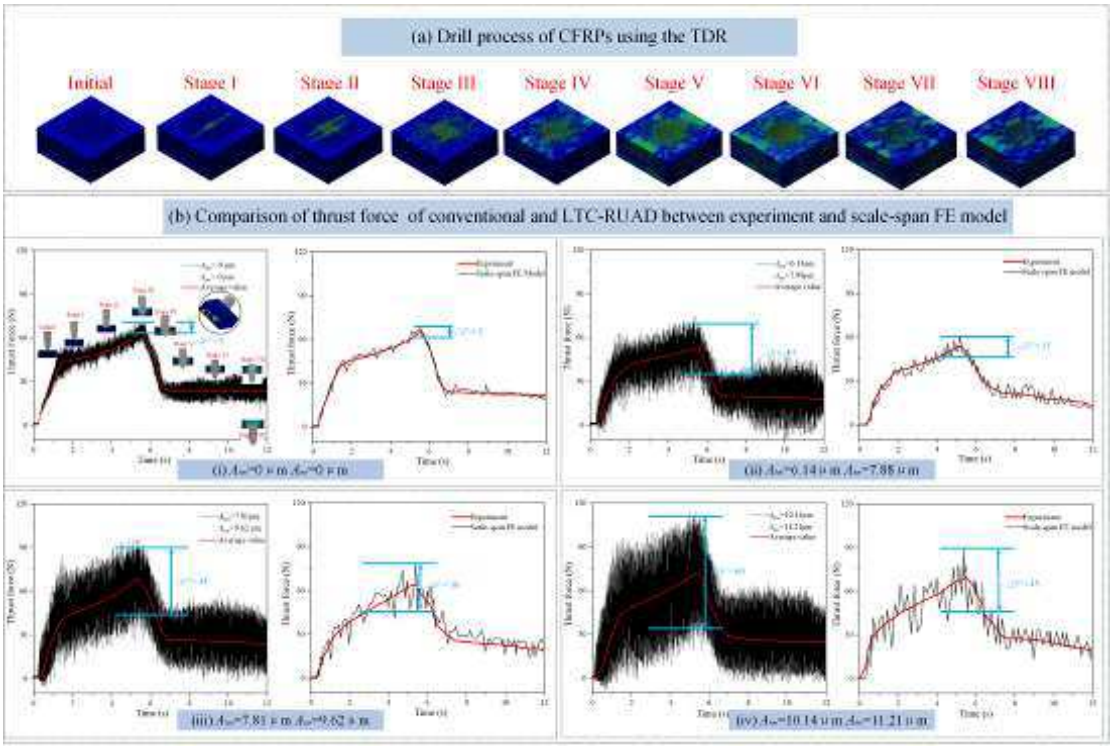

Fig.9 Comparison of the thrust force using CD and LTC-RUAD

Fig.10 presents the experimental and simulation results for the torque that adopts the LTC-RUAD with different UVA of the LTC vibration. Analogously, at the same period, there is also a great difference in the transient amplitude of variation change $\triangle T$. However, the vibration change of the torque can be clearly distinguish at different stages because there is no torsional vibration of the TDR bit in CD. According to the same reason as the explained by the thrust force, the vibration amplitude of the scale-span model is slight smaller than that of the experimental results because of the differences between the scale-span FE model and the microscopic cutting FE model.

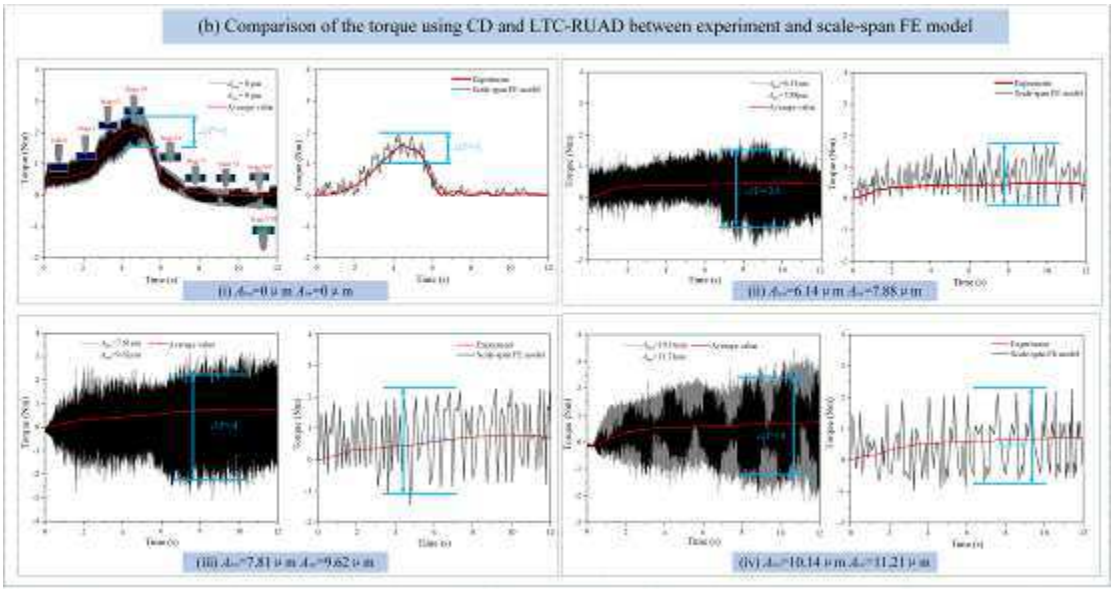

Fig.10 Setup showing the FE model of drilling CFRPs using LTC-RUAD

In order to evaluate the simulation results of the scale-span FE model accurately, the maximum average thrust force (obtained for the period of complete drill engagement) and the corresponding absolute percentage deviation are gathered among all the machining parameters, which is shown in Fig.11. The maximum average thrust force could be realistically predicted via the established scale-span FE model in drilling of CFRPs using LTC-RUAD, and the maximum deviation of the thrust force is only 7.58% among all process parameters compared with experiments. The simulation results and the experimental results showed that it could be maximumly reduced the maximum average thrust force when the UVA of the LTC vibration is approximately 7μm. The maximum average thrust force can be reduced by 27% in the case of the small UVA, especially in the case of high rotation speed, which is much lower than that of the CD.

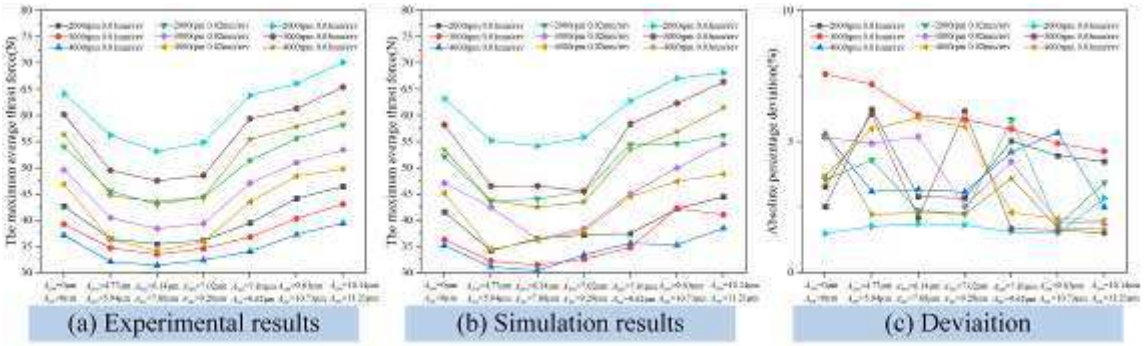

Fig.11 Comparison of the maximum average thrust force and deviation

Nonetheless, the value of thrust force among all the simulation results are almost smaller than the experimental results. The major reason is that the high frequency

vibration of the TDR bit leads to the premature failure of the contact elements in the scale-span FE model when the LTC-RUAD process is adopted. In addition, it should be noted that several factors could improve the accuracy of the scale-span FE model. Amongst these is the use of a more realistic friction model, inclusion of thermal effects and accounting for TDR wear effects.

4.2 Surface morphology

According to the research works by Cheng et al.[31], the micro-scale damage mechanism of UD-CFRPs is different when the different fiber cutting angles are adopted at microscopic, which is shown in Fig.12(b). Yet, in the drilling FE model, it can only show that the stress of the corresponding element is greater in the fiber orientation or elements are deleted because of the limitation of mesh size, which is shown in Fig.12(c) and Fig.13. Meanwhile, the hole-wall surface also appears different phenomena since the different lay-up angle, such as pits, tears, lateral extrusion and delamination, etc.

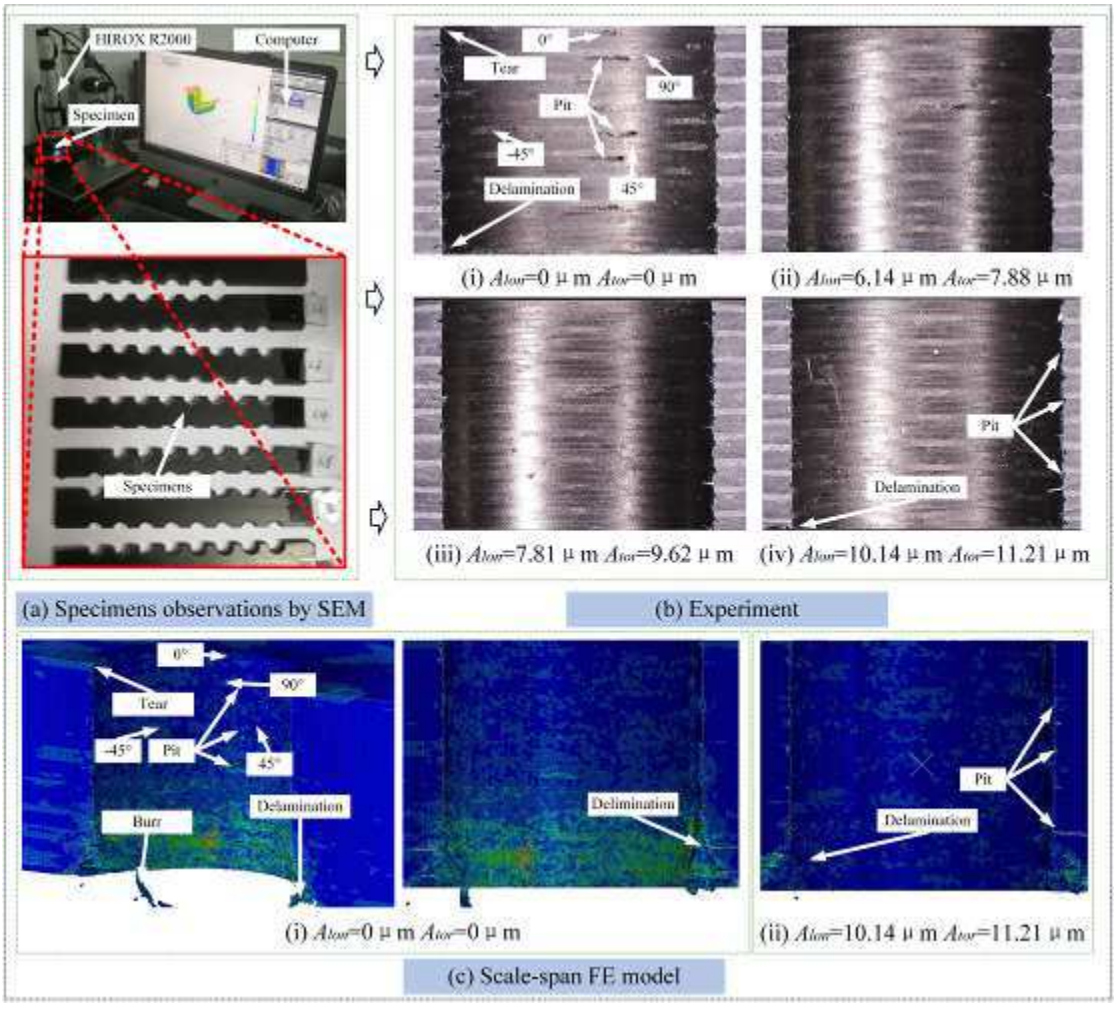

Fig.12 Comparison of the visualized damage phenomenon with CD and LTC-RUAD

Fig.12 shows the experimental and simulated results of the hole-wall surface morphology using CD and LTC-RUAD. In CD, due to there is lack of the vibration between the TDR bit and CFRPs workpieces, which causes the tear, pit and delamination in the different position according to the different lay-up of CFRPs. However, as shown in Fig.13, due to the effect of repeated vibration ironing using LTC-RUAD, the surface of the drilled hole is smoother than that using CD, and there are only some slight cracks according to the analysis of the cutting process at the micro-scale level. Since the damage of the scale-span FE model can only achieve material removal through element deletion or the corresponding stress value become larger, the elements that is located in the contact areas can be deleted quickly under the TDR of high-frequency vibration, namely, the fibers can be cut off quickly. Similarly, the elements of the FE model do not reach the maximum damage variable in CD, which promotes most of them are retained, whereas the corresponding stress is larger, especially in the bottom layers of CFRPs, which is shown in Fig.12(c).

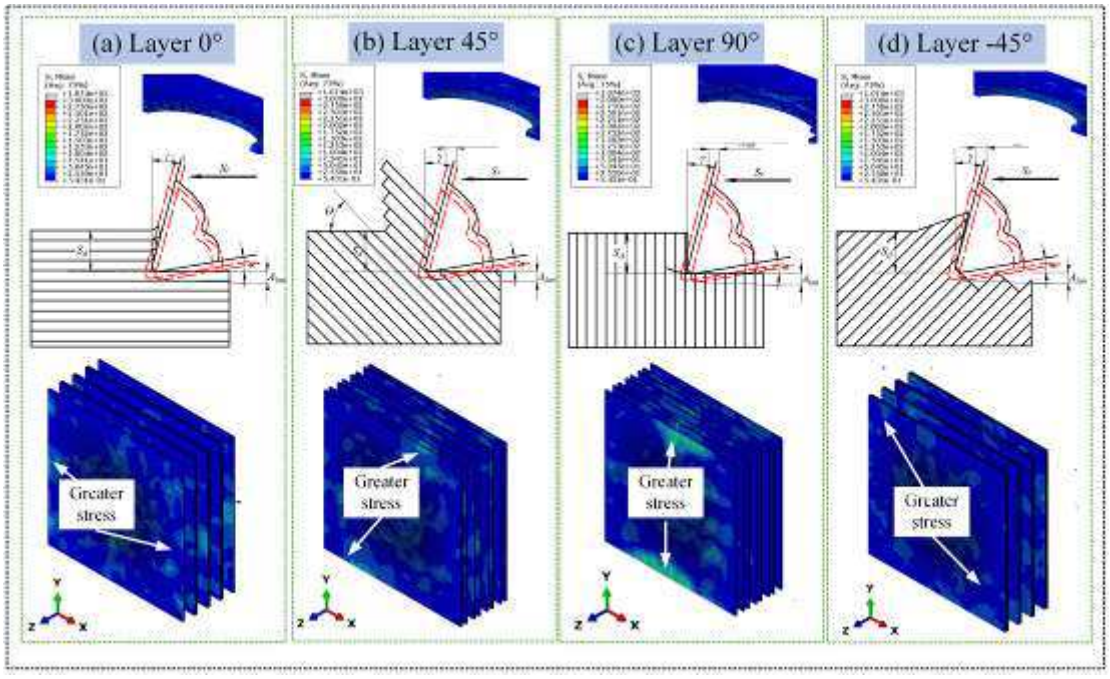

Fig.13 Damage defects suppression mechanism of CFRPs using LTC-RUAD

In addition, according to the comparative analysis of damage locations of each UD-CFRPs with different layer-up, the damaged positions at which there occurred tear, pits and delamination of the hole's surface are also consistent with the comparison of the scale-span drilling FE model and experiments using CD and LTC-RUAD. Therefore, the established scale-span drilling FE model can accurately predict the different kinds of the defects state of the CFRPs laminate prefabricated

hole's surface when the LTC-RUAD process is adopted.

4.3 Entry, exit damage and delamination

Fig.14 shows the experimental and simulated results of the hole-wall damage morphology at entry and exit using CD and LTC-RUAD. It can be seen that the entrance of the prefabricated hole is relatively flat, only a small amount of tear damage is occurred in experiments. Analogously, the scale-span FE model also shows the similar damage results. However, a large number of burr defect and tear damage are appeared in the exit of the hole. Similarly, burr damage phenomena are first simulated in the scale-span FE model, and the damage locations are almost the same, which is shown in Fig.14(a). Unfortunately, it is difficult to quantify the burr and tear damage owing to the fiber arrangement in species is random, and some initial damage may be existed in the species during preparing, such as microcrack, etc. Meanwhile, in the scale-span FE model that adopts the LTC-RUAD process, the hole-wall precision of the prefabricated hole has been improved obviously, and only minor tearing damage and delamination damage have appeared, which is shown in Fig.14(b).

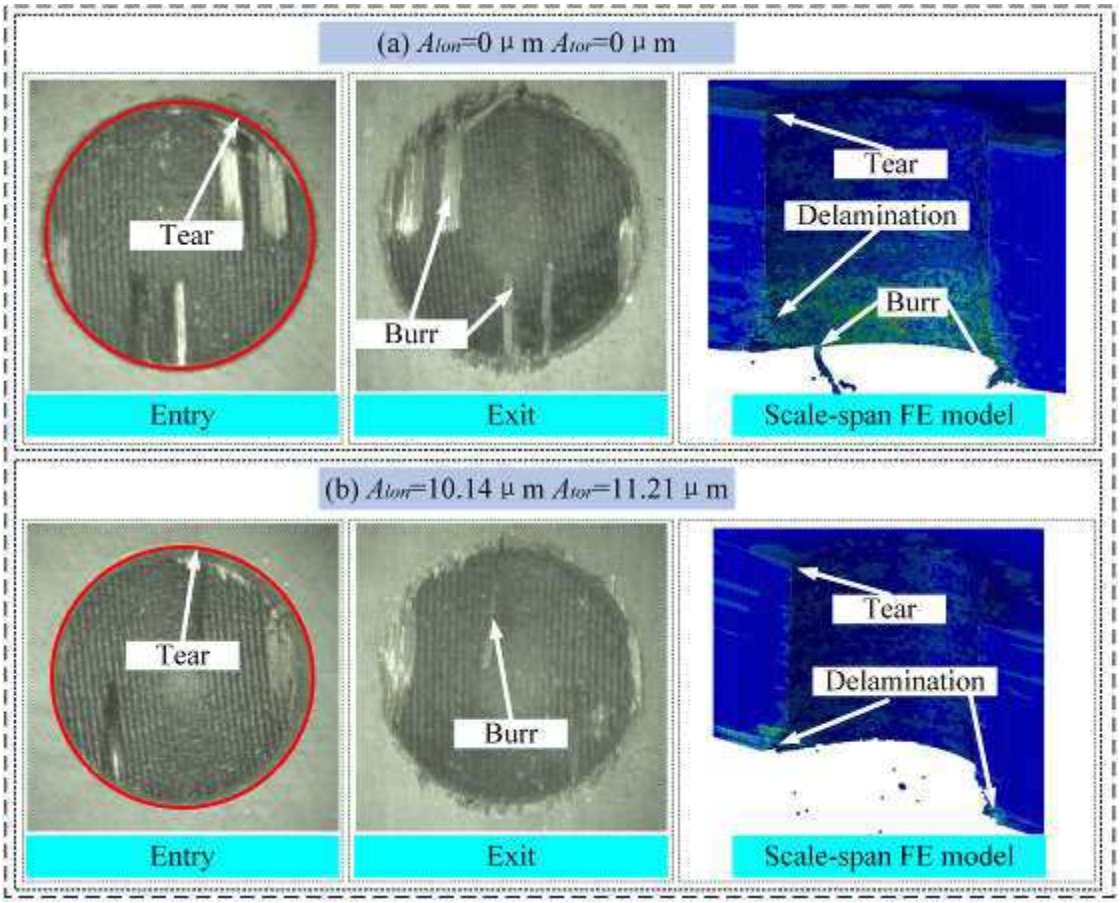

Fig.14 Comparison of the damage at the entry and exit with CD and LTC-RUAD

Delamination is a serious damage characterized by the separation of UD-CFRPs laminate caused by the thrust force. It often initiates at the hole edge and propagates along the fiber direction. The height of the delamination region is higher than the rest CFRPs [32]. In order to evaluate the simulation results of the scale-span FE model accurately and the delamination damage can inhibit the delamination using LTC-RUAD, a quantitative analysis of delamination factor at the exit of the hole is adopted in this study. According to Fig.15(b), the peripheral damage area is assumed as fan-shaped. It is defined as the ratio of the total peripheral damage area to the nominal hole area.

$$D_d = \left(\frac{A_d}{A_{nom}} - 1 \right) \% \tag{4}$$

where A_d denotes the total area of the delamination zone, A_{nom} denotes the nominal diameter area.

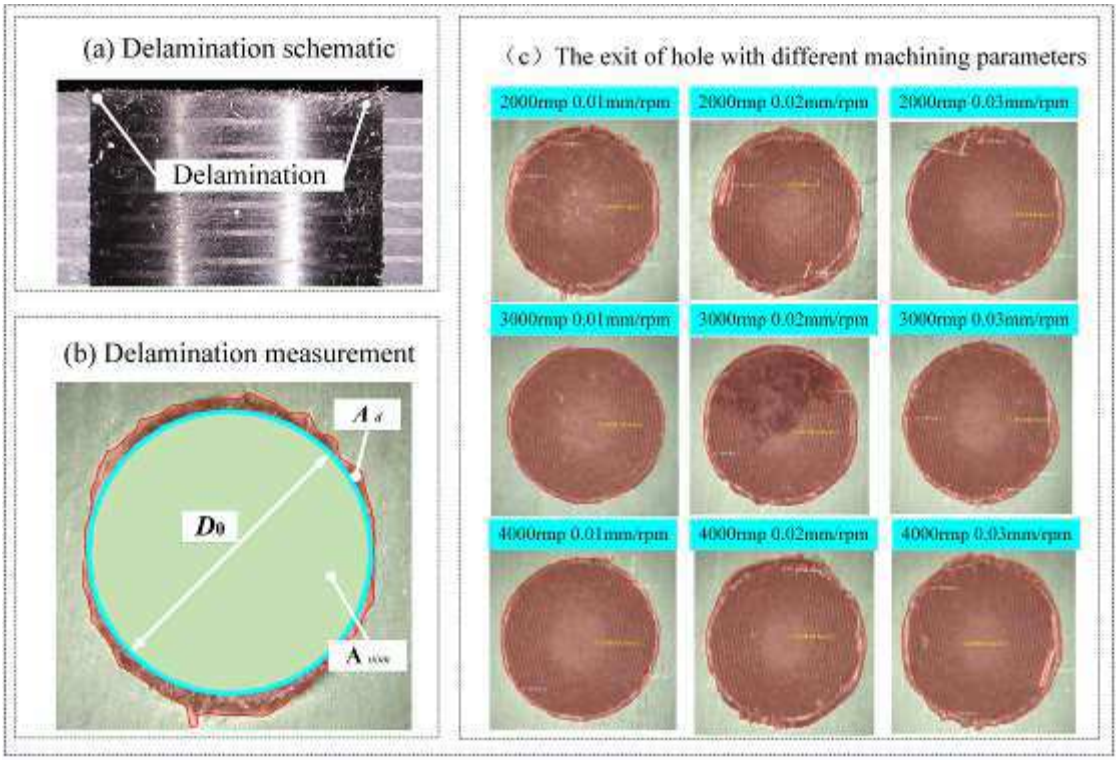

Fig.15 Measurement of delamination in experiments using LTC-RUAD

For the sake of obtain the value of A_d for the experimental measurement results from all the prefabricated holes, a portion of the uplift height at the exit of the hole is considered as delamination area of the specimens, while all the collecting and calculating works were done via SEM, which is shown in Fig.15(c). For the scale-span FE model, the ratio of total number of CEs before and after the drilling

simulation was calculated using an ABAQUS-Python code script, which is shown in Fig.16(c). According to the collected average experimental results and the simulation results from different process parameters and UVA, the corresponding delamination factor of drill exit and these absolute percentage deviations [2] are listed in Fig.17.

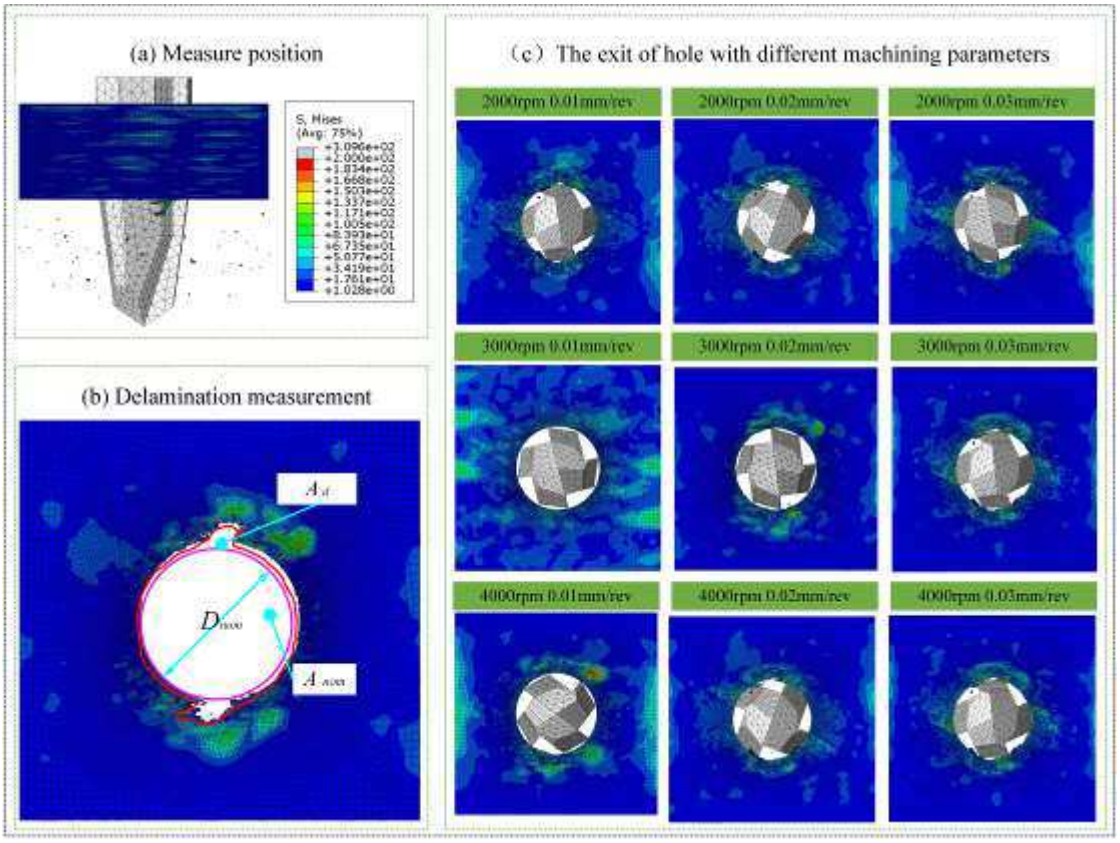

Fig.16 Measurement of delamination in LTC-RUAD scale-span FE model

As can be seen in Fig.17, the delamination damage behavior at the exit of hole could be realistically predicted via the established scale-span FE model in the drilling of CFRPs using CD and LTC-RUAD. The maximum and minimum deviation of the delamination factor is 15.69% and 0.309% compared with experiments, respectively. The dominant cause is that there is a material property deviation between the scale-span drilling FE model and experiments under the same machining parameters, followed by the deviation of the measurement devices. In addition, the other important reason is that the thermodynamic failure of elements in the drilling process is not taken into account in the established progressive failure theories model.

Although the deviation of the obtained simulation results is not regular, whereas the influence of the UVA for the suppression of the delamination is almost consistent via the analysis of the simulation results. The delamination factor shows a "concave" trend with the increase of UVA, especially at high rotational speed and low feed rate.

The reasons for this case are consistent with the maximum average thrust force, the UVA within the range of 7μm can be cut off the fiber quickly in the case of the high-frequency owing to it is equivalent to the diameter size of fiber. At the same time, it is also verified that the maximum average thrust force is the main factor causing the delamination [32].

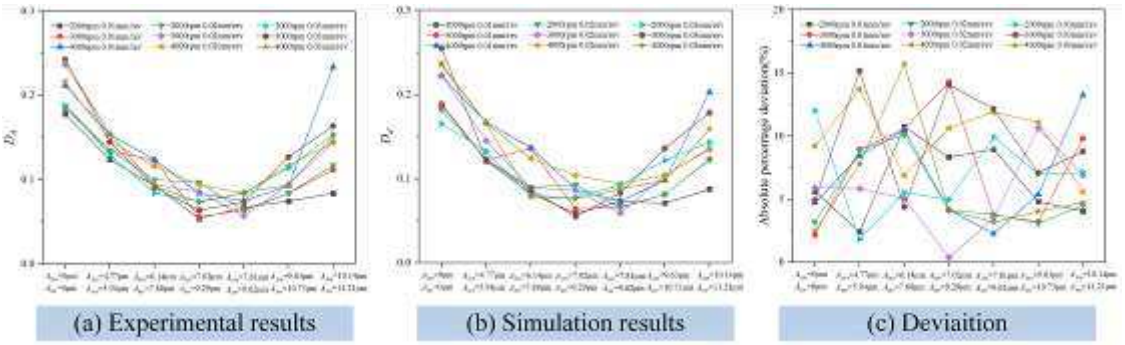

Fig.17 Comparison of the delamination and deviation

Finally, among all experimental and simulation results of scale-span FE model, the quality at the exit of the drilled hole is the best when adopting S_r=2000rpm, S_f=0.01mm/rev, A_{lon}=7.02μm and A_{tor}=9.29μm in LTC-RUAD. The delamination factor is only 0.054. The damage factors are reduced by 69.67% compared with CD. It is verified that adopting the LTC-RUAD process can greatly restrain the damage of precast holes in the drilling of CFRPs.

5.Conclusion

In this study, an experiment and scale-span numerical study of drilling in a T700S-12K/YP-H26 CFRPs was presented for both CD and LTC-RUAD process. A drilling experimental platform using LTC-RUAD was built based on the novel independently designed and manufactured LTC-RUAD vibration actuator, while drilling experiments involving T700S-12K/YP-H26 CFRPs specimens with different process parameters were carried out by modifying the UVA in the longitudinal and torsional directions. Then, a 3D scale-span FE simulation model of CD and LTC-RUAD which applied the different UVA using TDR was developed to find more details about the effects of machining quality of the holes. Finally, the defect suppression mechanism of CFRPs hole in LTC-RUAD were revealed via the simulation results from the perspectives of the thrust force and torque, surface morphology of the hole wall and delamination at the hole exit. The main conclusions are as follows:

(1) The predicted the thrust force and torque by the scale-span drilling FE model

is reasonable accuracy when compared to experimental results, and the maximum deviation are only 3.43% and 7.69%. And the maximum thrust force and torque that adopts LTC-RUAD is greater than that adopts CD. Nevertheless, the maximum average thrust force reduction was observed to be as high as 30% under certain drilling conditions.

(2) Different kinds of damage behavior of holes can be simulated truly in drilling of CFRP laminates using the TDR, such as the tear damage at drill entry, pits or lateral extrusion damage at drill surface and burr, tear and delamination at drill exit. The maximum thrust force and the delamination factor of the drilled hole shows a "concave" trend with the increase of the UVA. The corresponding parameters reaches the minimum value when the longitudinal UVA is approximately 7~9μm.

(3) In LTC-RUAD using the TDR, the quality at the exit of the drilled hole is the best when adopting S_r=2000rpm, S_f=0.01mm/rev, A_{lon}=7.02μm and A_{tor}=9.29μm in LTC-RUAD. The delamination factor is only 0.054. The damage factors are reduced by 69.67% compared with CD. In addition, the scale-span FE model was shown to replicated the drilling process effectively.

Acknowledgements

The authors would like to acknowledge the editors and the anonymous referees for their insightful comments.

Ethical approval

This article does not contain any studies with human participants performed by any of the authors.

Consent to participate

Work was conducted with no human test subjects.

Consent to publish

Work has consent to publish.

Authors' contributions

Yong Liu designed the study, performed the research, analysis data, and wrote the paper. **Qiannan Li** conducted experiments and data processing. **Zhenchao Qi** provided experimental condition and directed experiments. **Wenliang Chen** modified the paper.

Funding

The work reported herein is sponsored by the National Natural Science Foundation of China (51605221, 51875283), the Aeronautical Science Foundation of

China (2017ZE52052), and the National Commercial Aircraft Manufacturing Engineering Technology Research Center Innovation Foundation (COMAC-SFGS-2019-341). The authors would like to acknowledge the editors and the anonymous referees for their insightful comments.

Competing interests

Authors declare that they have no competing interests.

Availability of data and materials

The experimental and simulation data is transparency.

References

[1] Qi Z, Ge E, Yang J, Li F, Jin S (2021). Influence mechanism of multi-factor on the diameter of the stepped hole in the drilling of CFRP/Ti stacks, 113:923-933.

[2] Liu Y, Qi Z, Chen W, Wang X (2019) An approach to design high-performance unidirectional CFRPs based on a new sensitivity analysis model Composite Structures 224:111078.

[3] Abhishek K, Datta S, Mahapatra S S (2014). Optimization of thrust, torque, entry, and exist delamination factor during drilling of CFRP composites. The International Journal of Advanced Manufacturing Technology 76(1-4):401-416.

[4] Geng D, Liu Y, Shao Z, Lu Z, Cai J, Li X, Jiang X, Zhang D (2019) Delamination formation, evaluation and suppression during drilling of composite laminates: A review. Composite Structures 216: 168-186.

[5] Geng D, Teng Y, Liu Y, Shao Z, Jiang X, Zhang D (2019) Experimental study on drilling load and hole quality during rotary ultrasonic helical machining of small-diameter CFRP holes[J]. Journal of Materials Processing Technology 270:195-205.

[6] Chen Y, Su H, Qian N, He J, Ding K (2021) Ultrasonic vibration-assisted grinding of silicon carbide ceramics based on actual amplitude measurement: Grinding force and surface quality. Ceramics International 47:15433-15441.

[7] Zhang D, Wang H, Burks A R, Cong W (2020) Delamination in rotary ultrasonic machining of CFRP composites: finite element analysis and experimental implementation. The International Journal of Advanced Manufacturing Technology 107(1):1-12.

[8] Wang J, Zhang J, Feng P, Ping Q (2018) Feasibility Study of Longitudinal Torsional Coupled Rotary Ultrasonic Machining of Brittle Material. Journal of

Manufacturing Science & Engineering 140(5): 051008.

[9] Wang J, Feng P, Zhang J, Guo P (2018) Reducing cutting force in rotary ultrasonic drilling of ceramic matrix composites with longitudinal-torsional coupled vibration. Manufacturing Letters 18:1-5.

[10] Sadek A, Attia M H, Meshreki M, Shi B (2013) Characterization and optimization of vibration-assisted drilling of fibre reinforced epoxy laminates. CIRP Annals - Manufacturing Technology 62(1):91-94.

[11] Cong W L, Pei Z J, Sun X, Zhang C (2014) Rotary ultrasonic machining of CFRP: A mechanistic predictive model for cutting force. Ultrasonics 54(2):663-675.

[12] Wang H, Ning F, Li Y, Hu Y, Cong W (2019) Scratching-induced Surface Characteristics and Material Removal Mechanisms in Rotary Ultrasonic Surface Machining of CFRP. Ultrasonics 97:19-28.

[13] Wang H, Hu Y, Cong W, Burks A (2019) Rotary ultrasonic machining of carbon fiber–reinforced plastic composites: effects of ultrasonic frequency. The International Journal of Advanced Manufacturing Technology, 2019, 104(3): 3759–3772.

[14] Thomas P N H, Babitsky V I (2017) Experiments and simulations on ultrasonically assisted drilling. Journal of Sound & Vibration 308(3-5):815-830.

[15] Makhdum F, Phadnis V A, Roy A, Silberschmidt V (2014) Effect of ultrasonically-assisted drilling on carbon-fibre-reinforced plastics. Journal of Sound and Vibration 333(23):5939-5952.

[16] Asami T, Miura H (2015) Study of ultrasonic machining using longitudinal and torsional vibration, 2015 IEEE International Ultrasonics Symposium (IUS). IEEE.

[17] Lotfi M, Amini S (2016) Effect of ultrasonic vibration on frictional behavior of tool–chip interface: Finite element analysis and experimental study. Proceedings of the Institution of Mechanical Engineers Part B Journal of Engineering Manufacture (7): 1212-1220.

[18] Phadnis V A, Makhdum F, Roy A, Silberschmidt V (2012) Experimental and Numerical Investigations in Conventional and Ultrasonically Assisted Drilling of CFRP Laminate. Procedia Cirp 1(7):455-459.

[19] Phadnis V A, Roy A, Silberschmidt V V (2013) A Finite Element Model of Ultrasonically Assisted Drilling in Carbon/Epoxy Composites. Procedia CIRP 8(1):141-146.

[20] Gomes G F, Diniz C A, Da Cunha S S, Ancelotti AC (2017) Design optimization of composite prosthetic tubes using GA-ANN algorithm considering Tsai-Wu failure criteria. Journal of Failure Analysis & Prevention 17:740-749.

[21] Hashin Z, Rotem A (1973) A Fatigue failure criterion for fiber reinforced materials. Journal of Composite Materials 7(4):448-464.

[22] Hashin, Z (1981) Fatigue failure criteria for unidirectional fiber composites. Journal of Applied Mechanics 48(4):846.

[23] A. Puck, H (2002) Schürmann. Failure analysis of FRP laminates by means of physically based phenomenological models. Composites Science and Technology 62:1633-1662.

[24] Chang F K, Chang K Y (1987) A progressive damage model for laminated composites containing stress concentrations. Journal of Composite Materials, 21(9):834-855.

[25] Ma X, Li Y, Gu Y, Li M, Zhang Z (2014) Numerical simulation of prepreg resin impregnation effect in vacuum-assisted resin infusion/prepreg co-curing process. Journal of Reinforced Plastics and Composites 33:2265-73.

[26] Tsao C C, Hocheng H (2008) Evaluation of thrust force and surface roughness in drilling composite material using Taguchi analysis and neural network. Journal of Materials Processing Technology 203(1-3):342-348.

[27] Wang F, Qian B, Jia Z, Cheng D, Fu R (2018) Effects of cooling position on tool wear reduction of secondary cutting edge corner of one-shot drill bit in drilling CFRP. International Journal of Advanced Manufacturing Technology 94:4277-4287.

[28] Liu Y, Li QN, Qi Z, Chen W. Scale-span modelling of dynamic progressive failure and experimental study in drilling CFRPs with a tapered drill-reamer. Composite Structures (COMSTR-D-20-02100 Under review)

[29] Zhenchao Qi, Yong Liu, Wenliang Chen (2019) An approach to predict the mechanical properties of CFRP based on cross-scale simulation. Composite Structures 210:339-47.

[30] Ducobu F, Rivière-Lorphèvre, E, Filippi E (2015) On the introduction of adaptive mass scaling in a finite element model of Ti6Al4V orthogonal cutting. Simulation Modelling Practice & Theory 53:1-14.

[31] Chen L, Zhang K, Hui C, Qi Z, Meng Q (2017) A cutting force predicting model in orthogonal machining of unidirectional CFRP for entire range of fiber

orientation. The International Journal of Advanced Manufacturing Technology 89(1-4):1-14.

[32] Faraz A, Biermann D, Weinert K (2009) Cutting edge rounding: An innovative tool wear criterion in drilling CFRP composite laminates. International Journal of Machine Tools & Manufacture 49(15):1185-1196.

Figure caption

Table caption

Figures

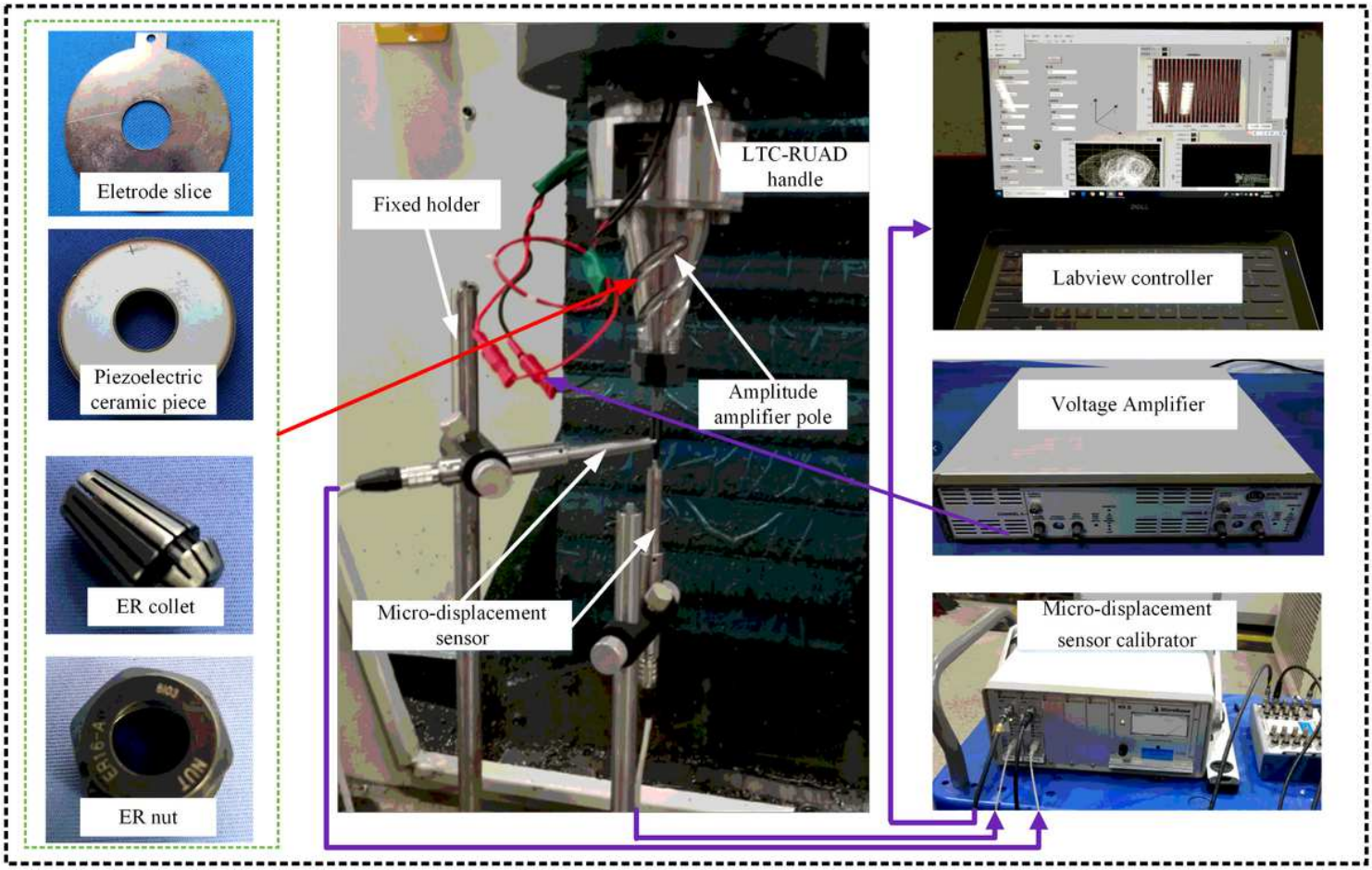

Figure 1

LTC-RUAD handle and ultrasonic amplitude calibration

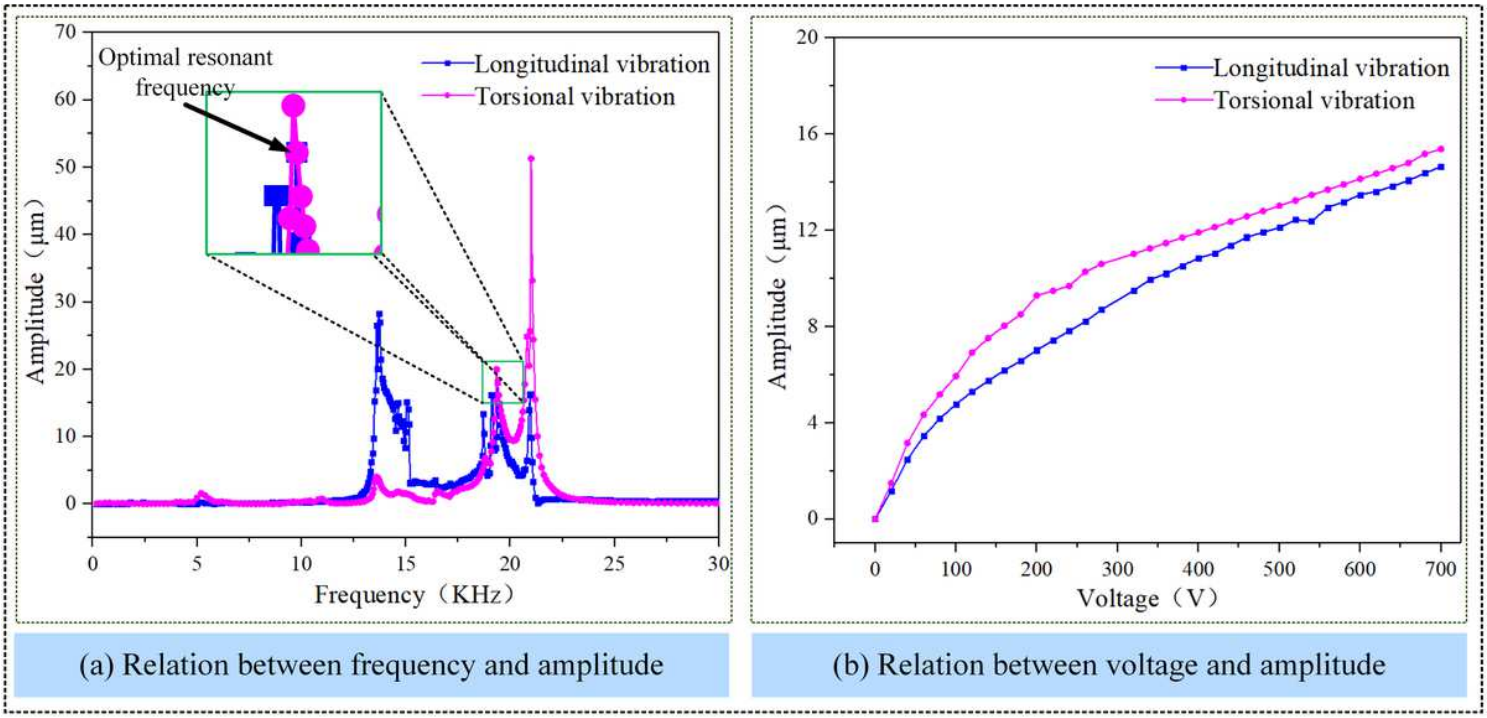

Figure 2

Frequency-amplitude and voltage-amplitude diagram

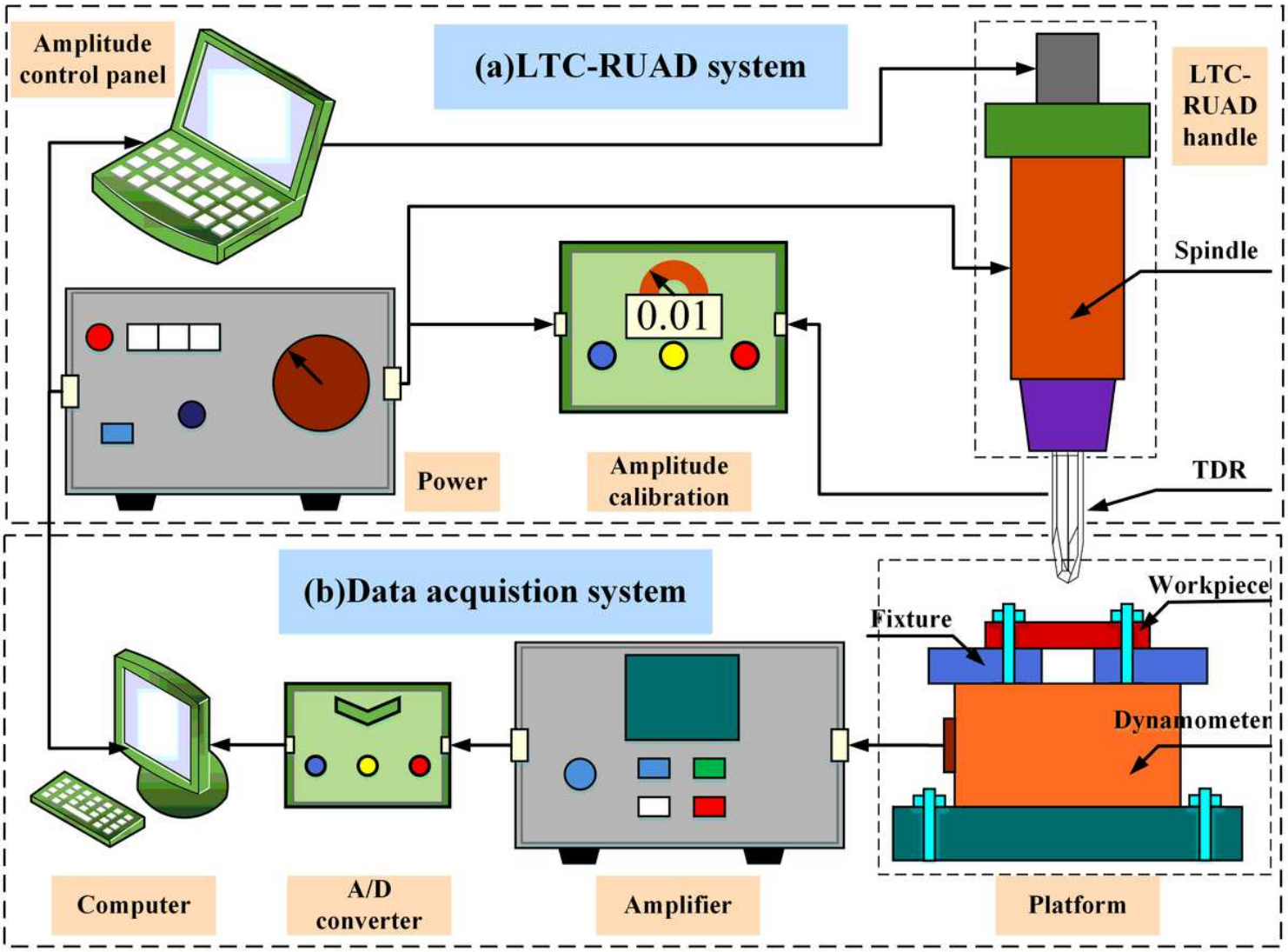

Figure 3

Defect suppression mechanism of the drilling hole using the TDR bit

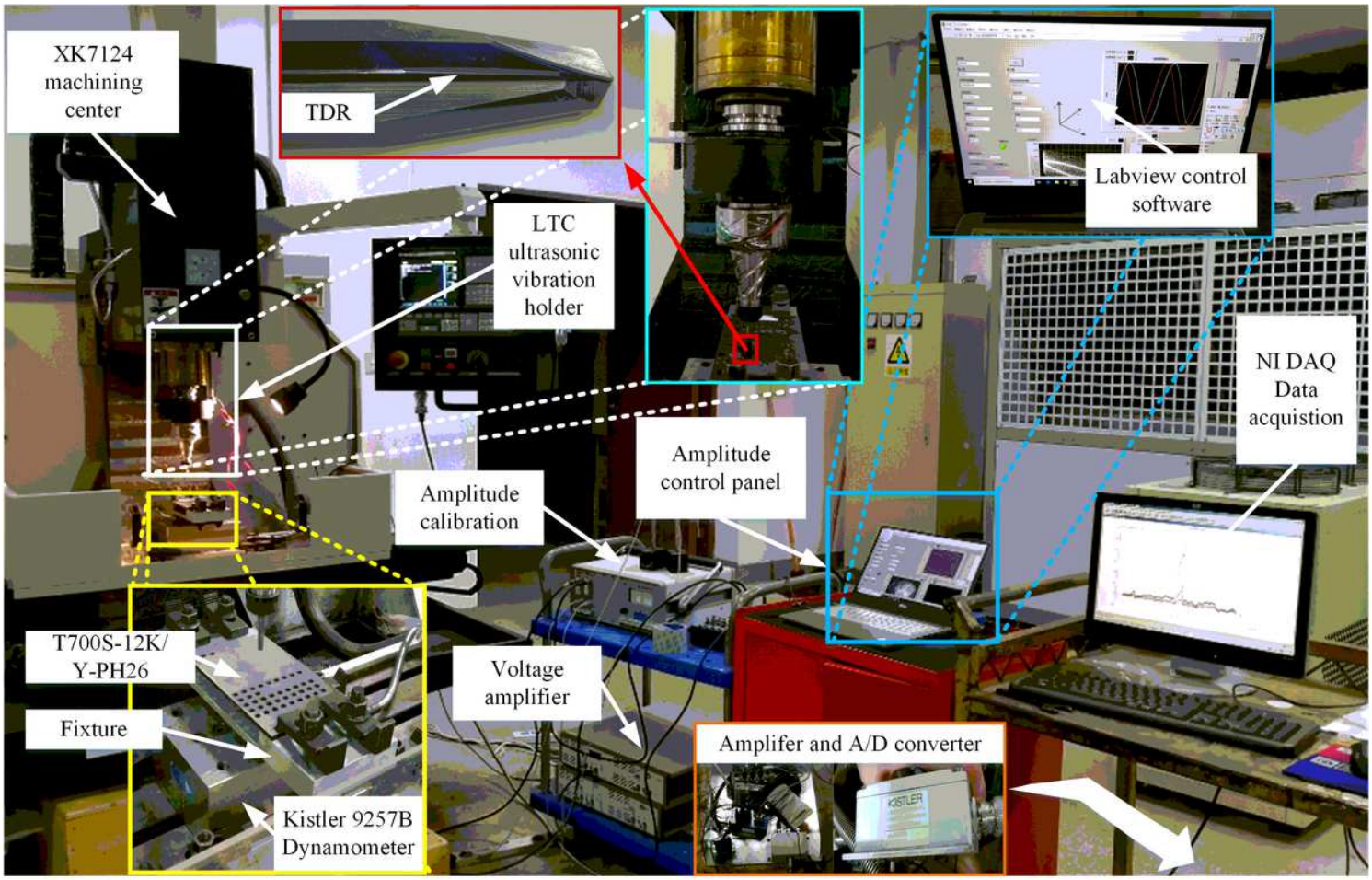

Figure 4

LTC-RUAD handle and ultrasonic amplitude calibration

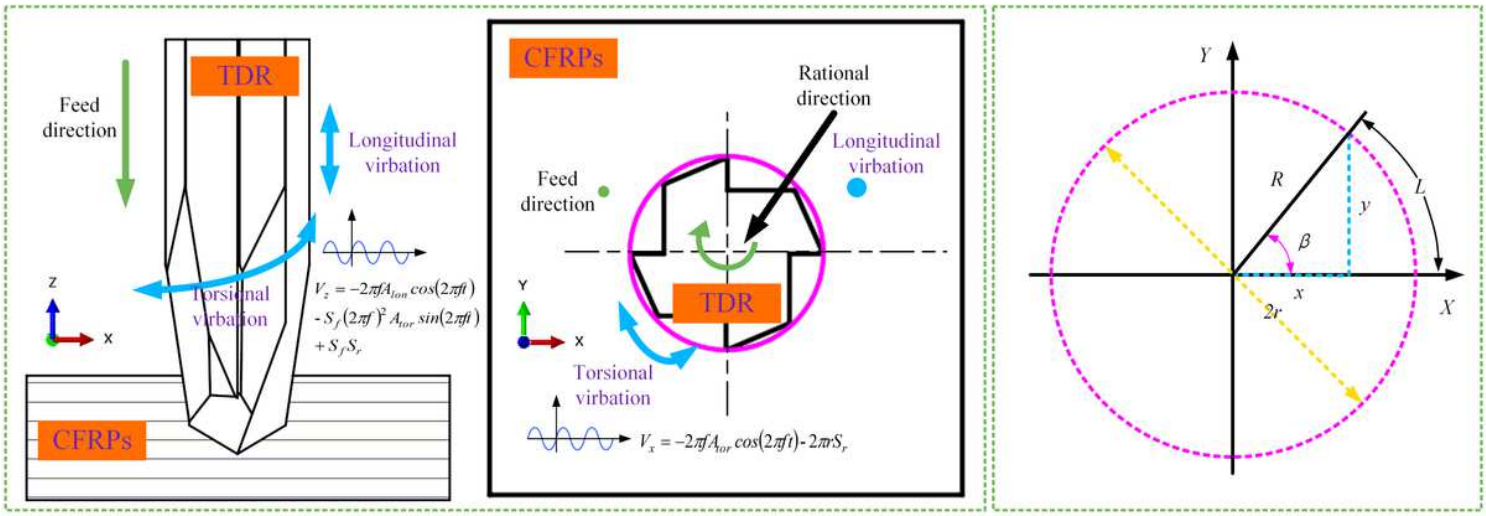

Figure 5

Illustration of LTC-RUAD using TDR

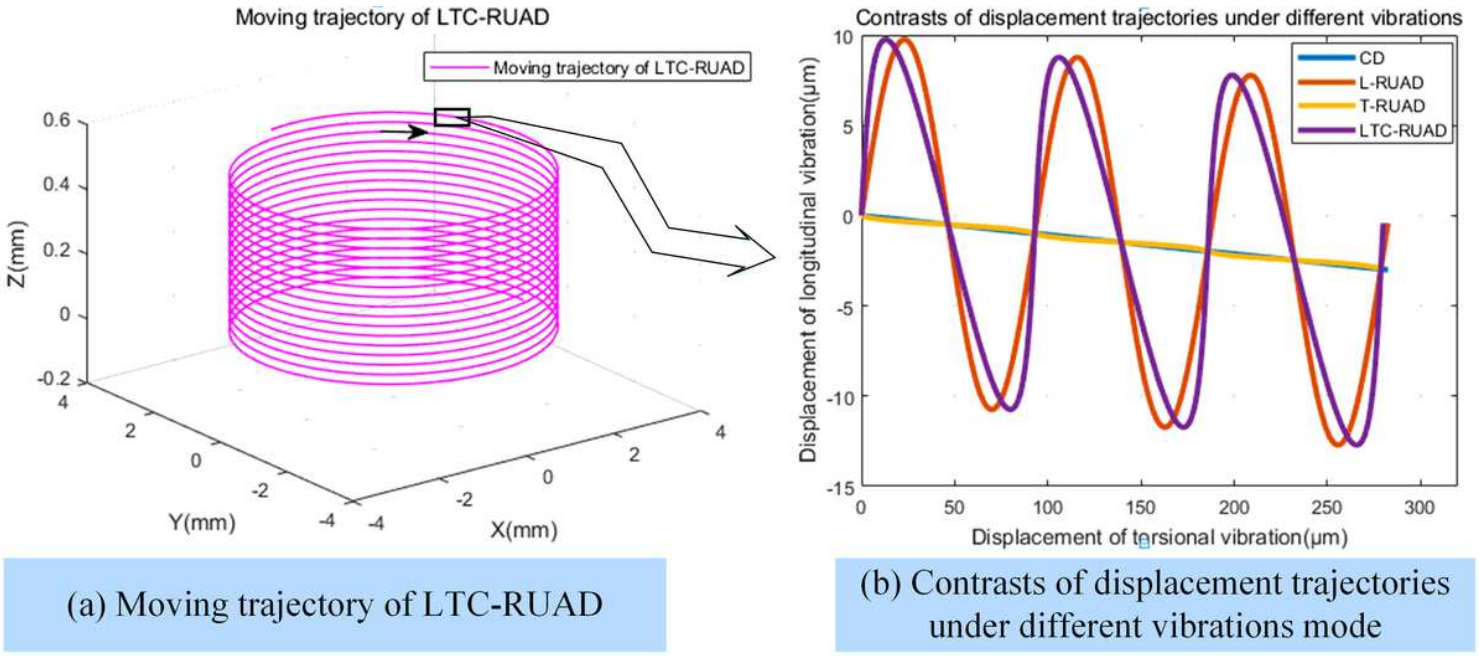

Figure 6

Moving trajectory of TDR

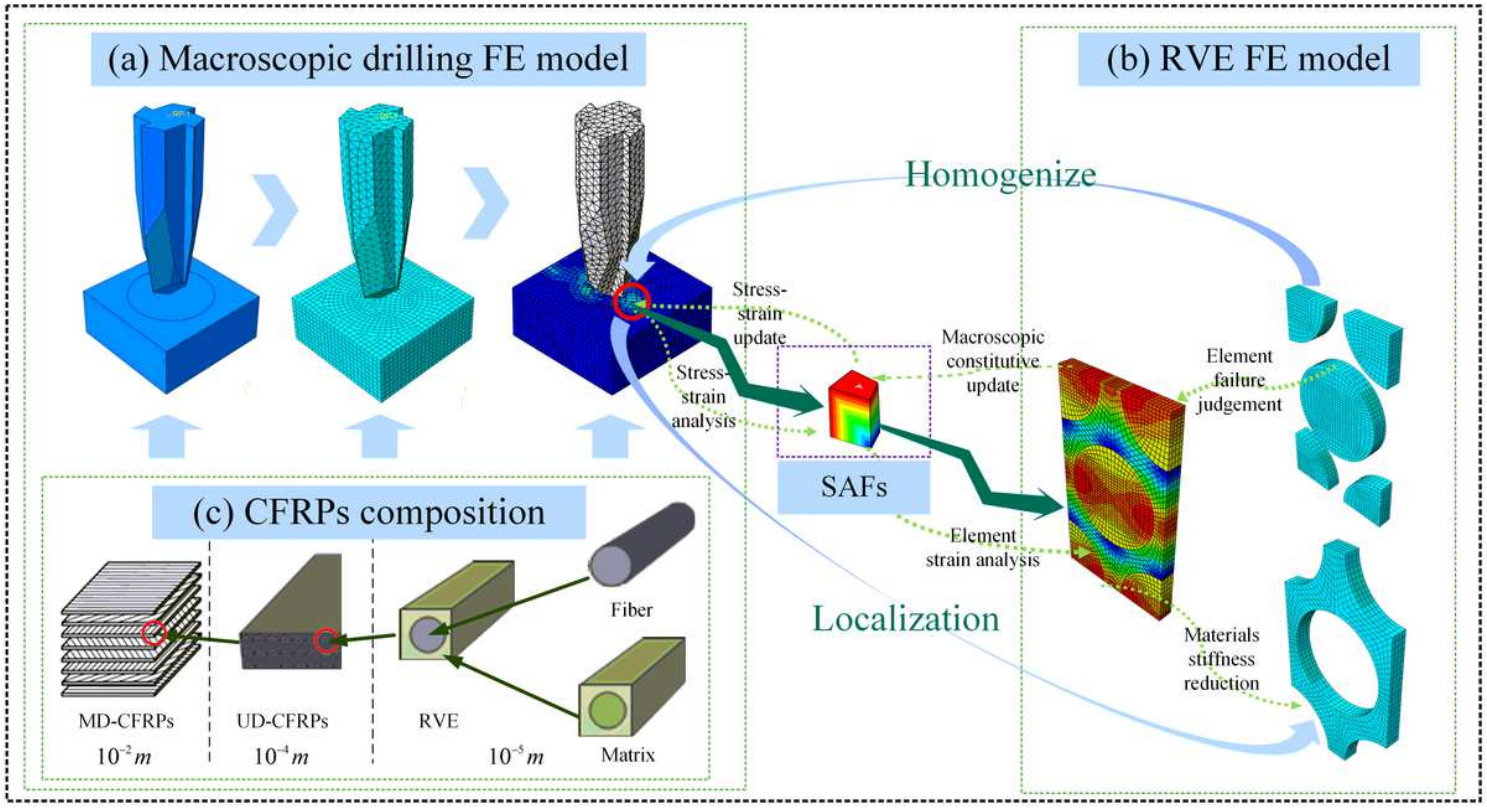

Figure 7

Scale-span FE drilling schematic diagram

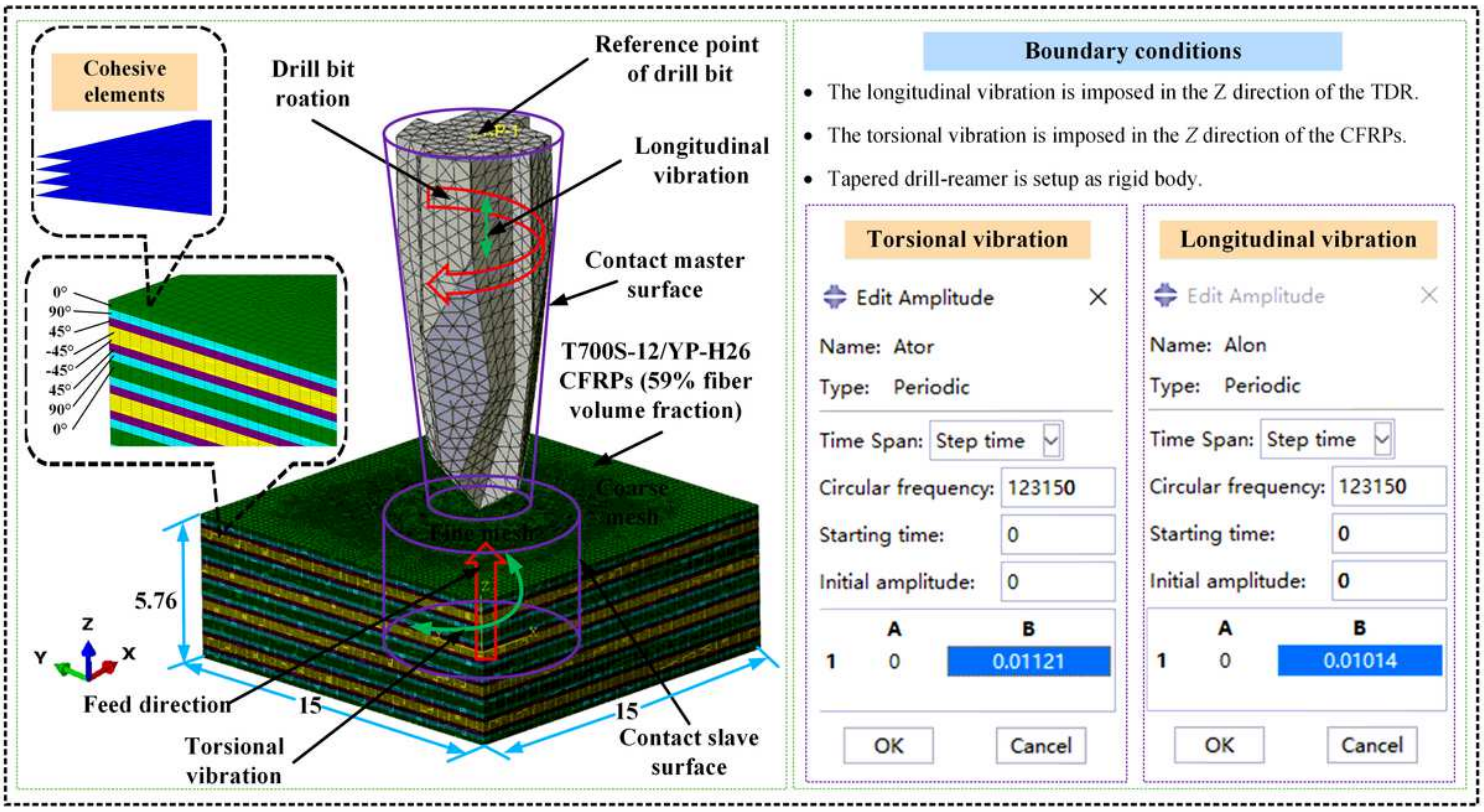

Figure 8

Setup showing the FE model of drilling CFRPs using LTC-RUAD

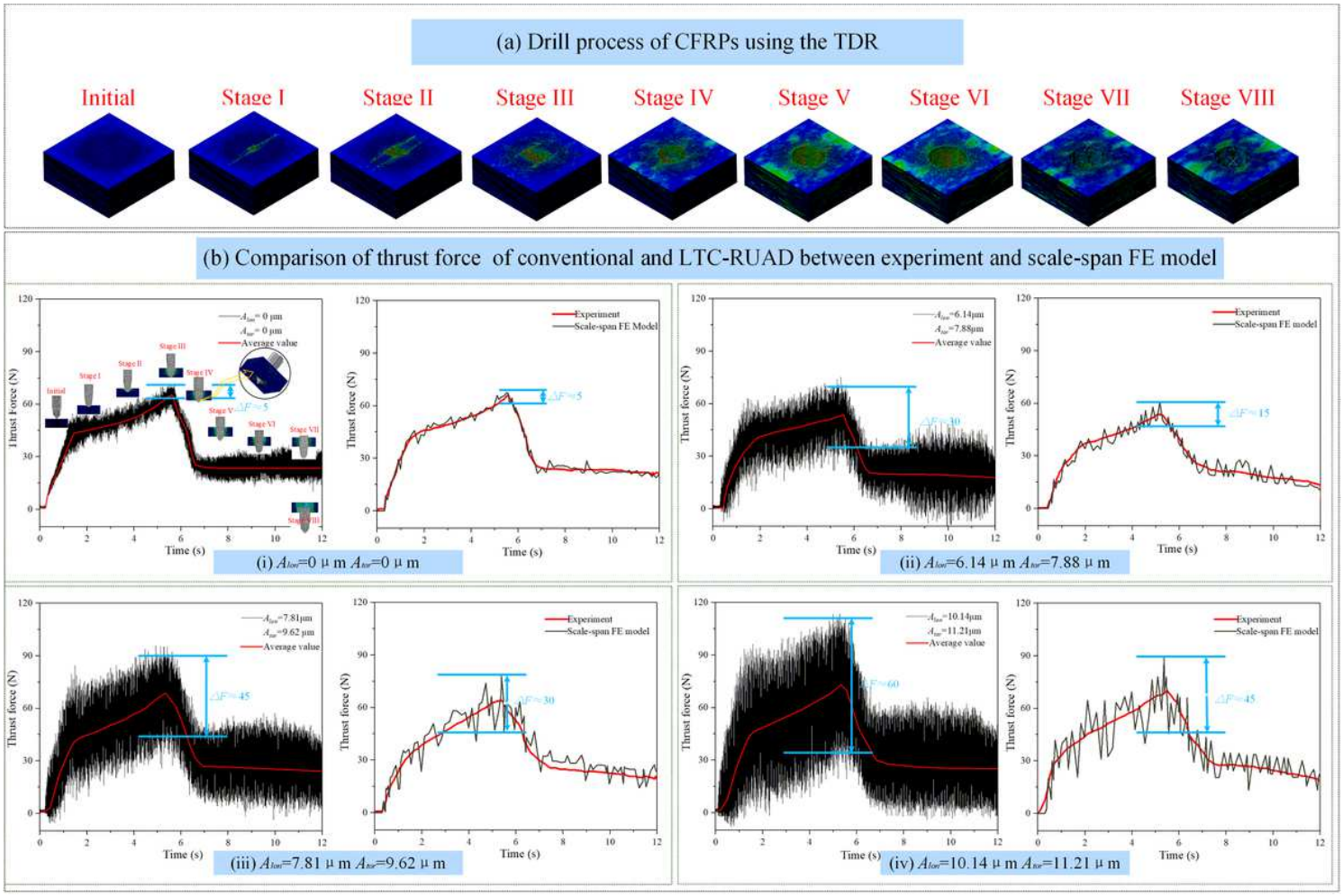

Figure 9

Comparison of the thrust force using CD and LTC-RUAD

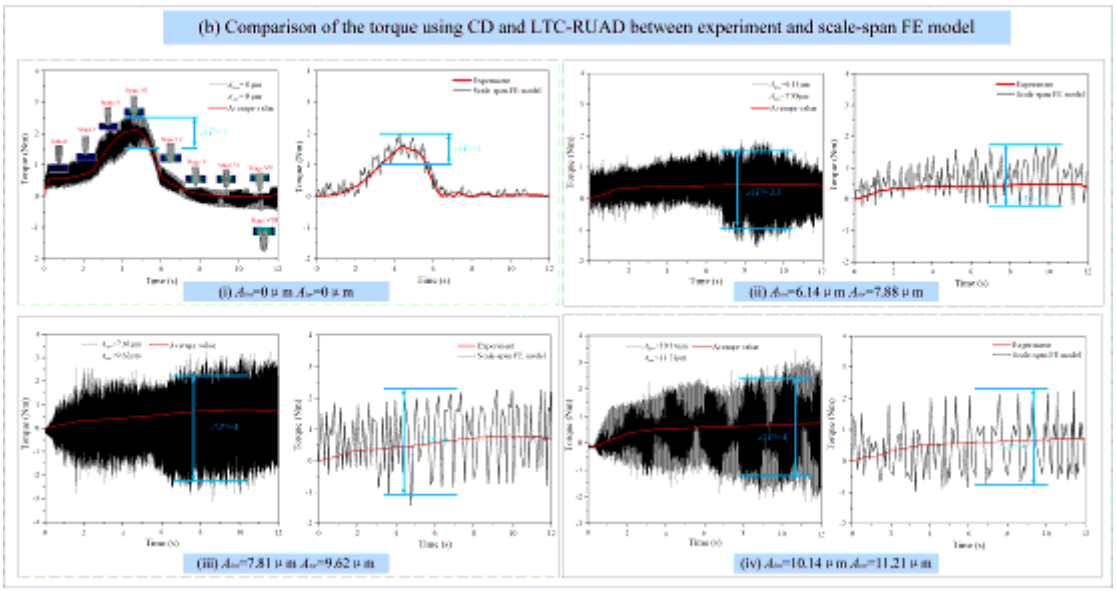

Figure 10

Setup showing the FE model of drilling CFRPs using LTC-RUAD

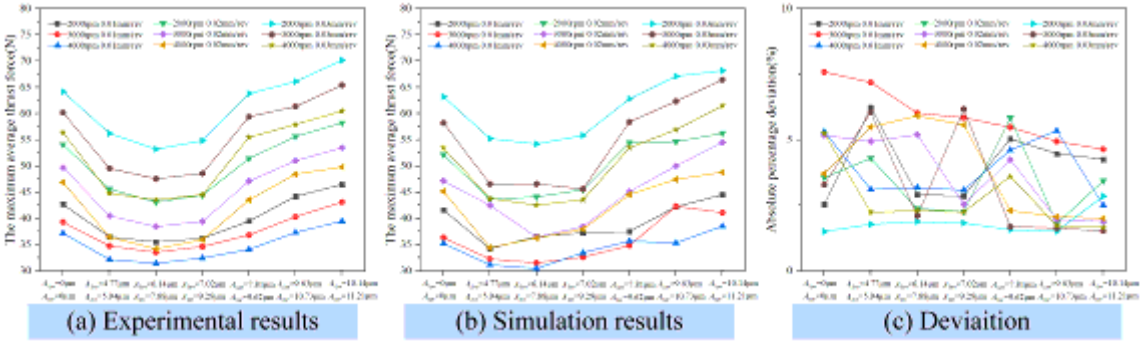

Figure 11

Comparison of the maximum average thrust force and deviation

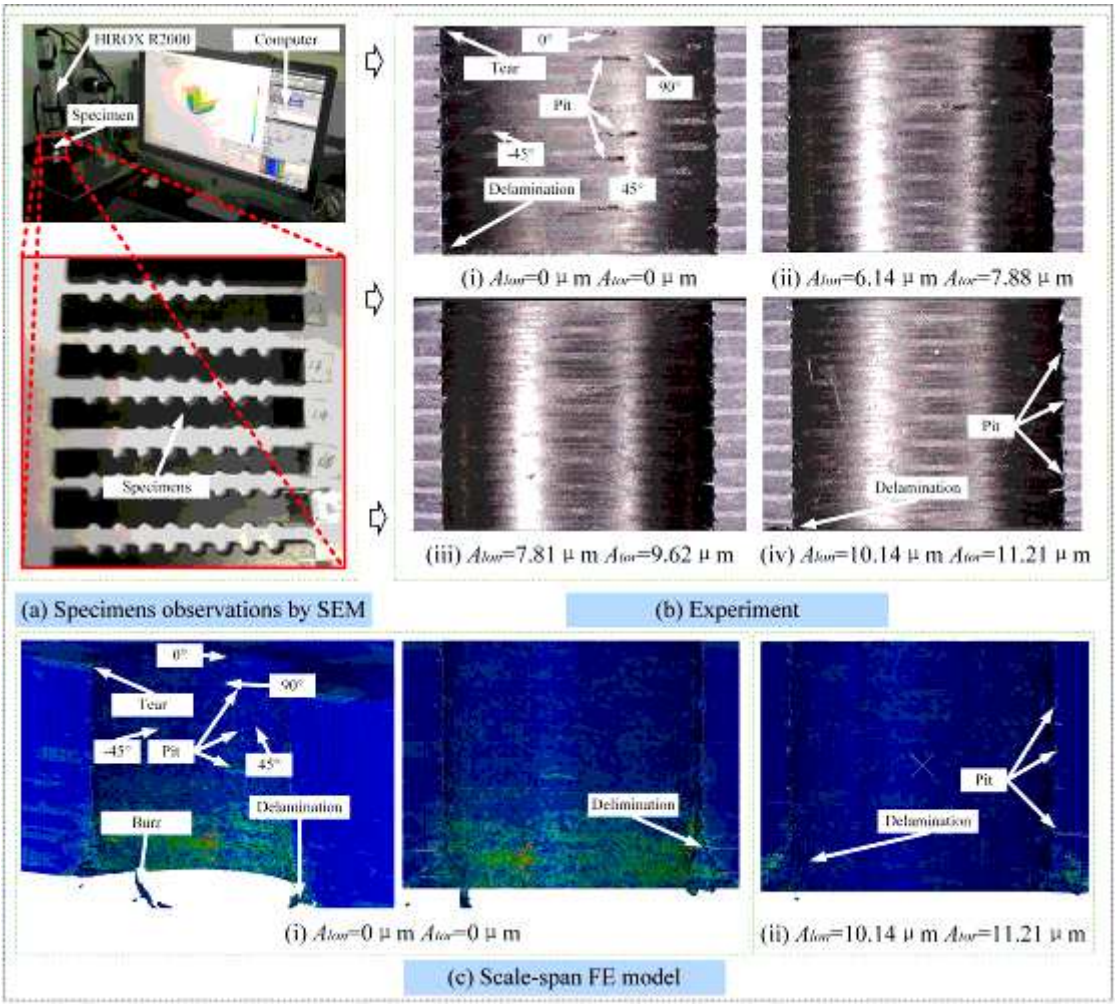

Figure 12

Comparison of the visualized damage phenomenon with CD and LTC-RUAD

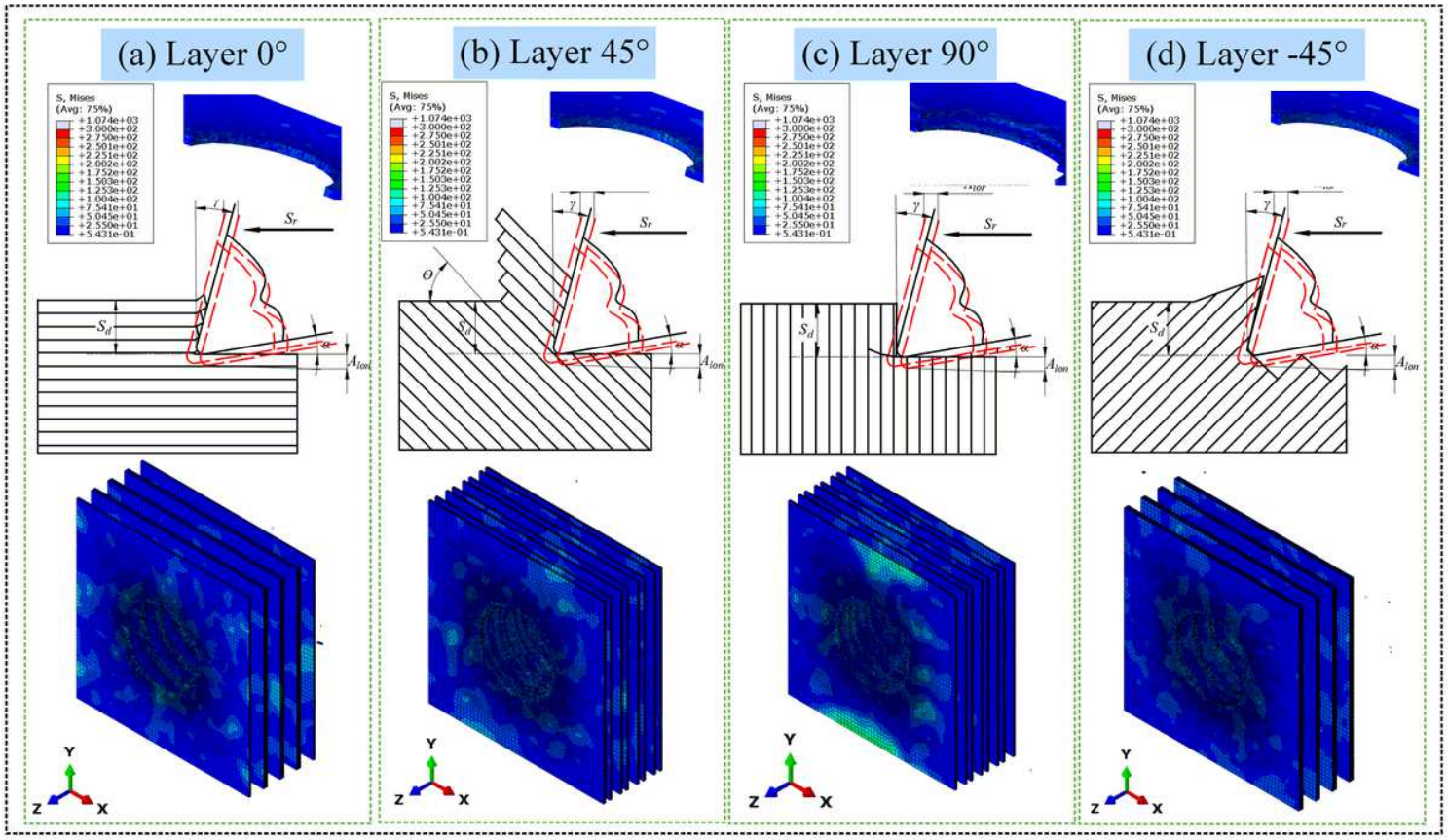

Figure 13

Damage defects suppression mechanism of CFRPs using LTC-RUAD

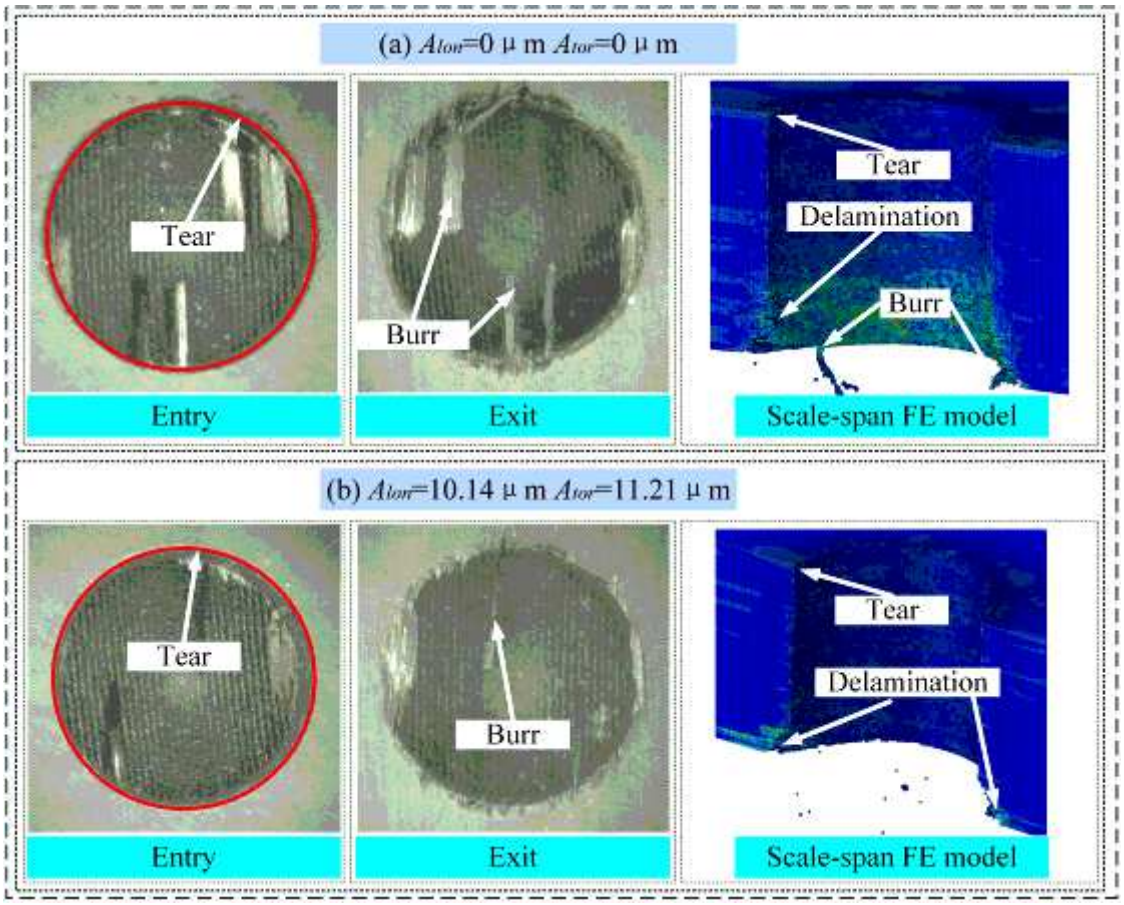

Figure 14

Comparison of the damage at the entry and exit with CD and LTC-RUAD

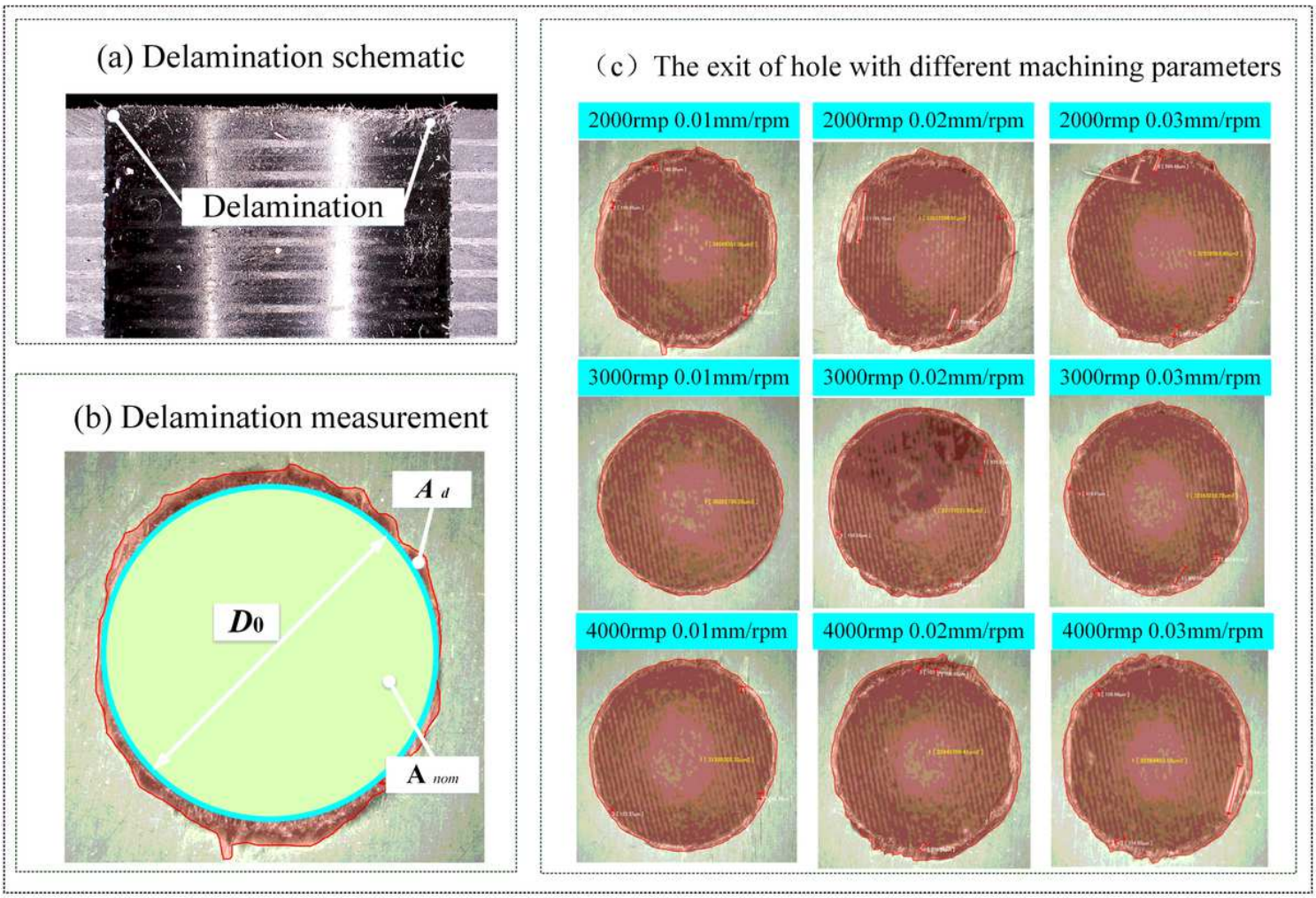

Figure 15

Measurement of delamination in experiments using LTC-RUAD

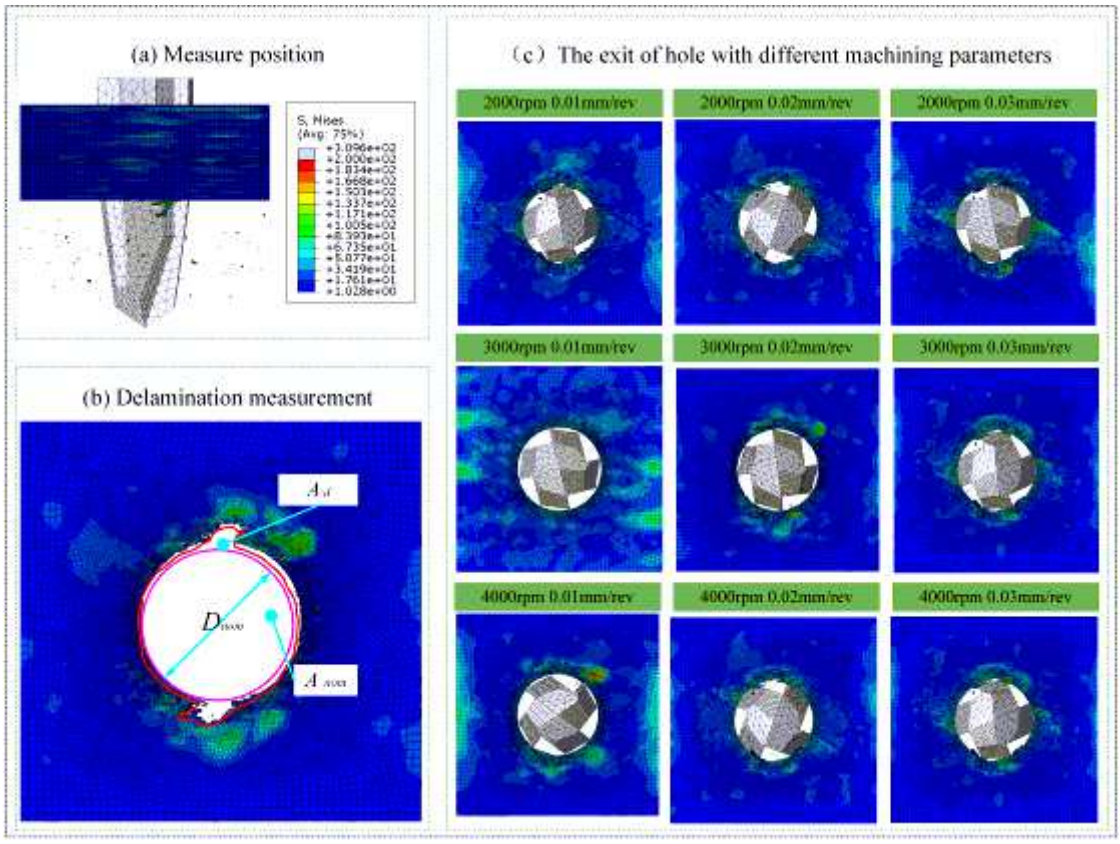

Figure 16

Measurement of delamination in LTC-RUAD scale-span FE model

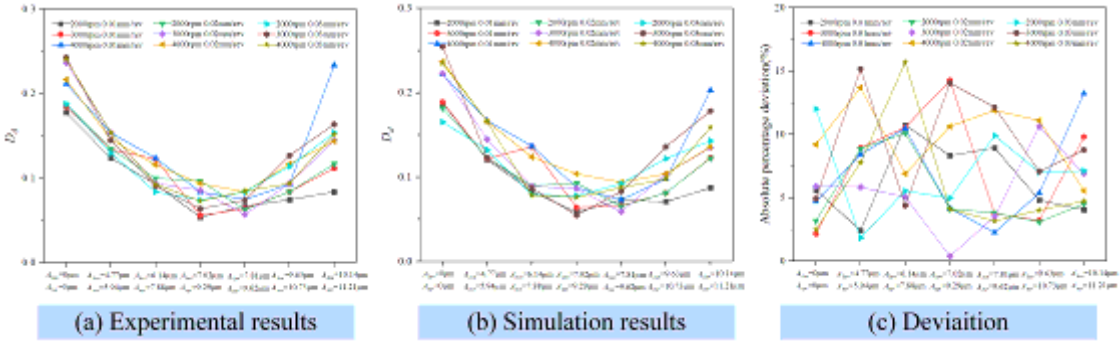

Figure 17

Comparison of the delamination and deviation